



HAL
open science

Evolution and final closure of the Mongol-Okhotsk Ocean

Pan Zhao, Bei Xu, Yan Chen

► **To cite this version:**

Pan Zhao, Bei Xu, Yan Chen. Evolution and final closure of the Mongol-Okhotsk Ocean. Science China Earth Sciences, 2023, 66 (11), pp.2497-2513. 10.1007/s11430-023-1165-9 . insu-04359838

HAL Id: insu-04359838

<https://insu.hal.science/insu-04359838v1>

Submitted on 8 Jan 2024

HAL is a multi-disciplinary open access archive for the deposit and dissemination of scientific research documents, whether they are published or not. The documents may come from teaching and research institutions in France or abroad, or from public or private research centers.

L'archive ouverte pluridisciplinaire **HAL**, est destinée au dépôt et à la diffusion de documents scientifiques de niveau recherche, publiés ou non, émanant des établissements d'enseignement et de recherche français ou étrangers, des laboratoires publics ou privés.

1 Evolution and final closure of the Mongol-Okhotsk Ocean

2 Pan Zhao^{1*}, Bei Xu², Yan Chen³

3
4 1. State Key Laboratory of Lithospheric Evolution, Institute of Geology and
5 Geophysics, Chinese Academy of Sciences, Beijing 100029, China

6 2. Hebei Key Laboratory of Strategic Critical Mineral Resources, Hebei GEO
7 University, Shijiazhuang 050031, China

8 3. Univ. Orléans, CNRS, BRGM, ISTO, UMR 7327, F-45071, Orléans, France

9 *Corresponding author E-mail: panzhao@mail.iggcas.ac.cn

10 11 12 **Abstract:**

13 Mongol-Okhotsk Orogenic Belt is the last main orogen that constructs modern
14 tectonic framework of northeastern Asia. It has recorded the long-term evolution of the
15 Mongol-Okhotsk Ocean (MOO) from its Early Paleozoic initial opening, through the
16 Late Paleozoic-Early Mesozoic subduction, to its Mesozoic final closure, leading to the
17 amalgamation of the Siberian Craton (SIB) and North China-Amuria Block (NCC-
18 AMB). Opening of the MOO can be traced to the early stage of the Early Paleozoic.
19 Northward subduction of the Mongol-Okhotsk oceanic slab beneath the southern
20 margin of the SIB initiated in the Silurian, whereas the southward subduction beneath
21 the northern margin of the NCC-AMB started in the Late Devonian. The bidirectional
22 subduction of the Mongol-Okhotsk oceanic slab resulted in pulse arc magmatism, with
23 three main peaks in the earliest Carboniferous, Late Permian and Late Triassic-Early
24 Jurassic. In the Late Triassic, the collision between the AMB and Western Mongolian
25 Blocks led to the bending of the Western Mongolian Blocks, which caused the initial
26 closure of the MOO in its western segment. Due to the clockwise rotation of the SIB
27 and counterclockwise rotation of the NCC-AMB, the MOO showed a scissor-like
28 closure from west to east. The final closure of the MOO occurred in the Middle-Late
29 Jurassic, which also resulted in the formation of the Mongol Orocline. Since then, the

30 amalgamation of blocks in northeastern Asia has finished, and the northeastern Asian
31 continent went into the intraplate evolutionary stage.

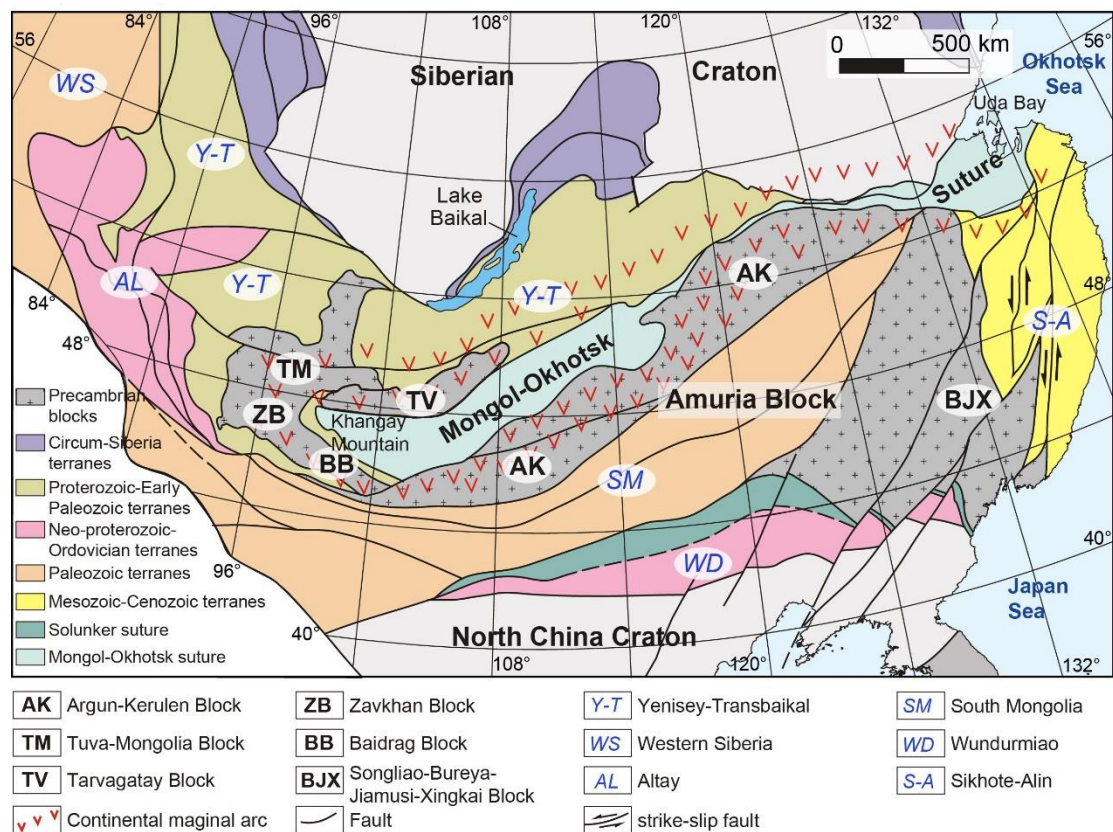
32

33 **Keywords:** Northeastern Asia; Mongol-Okhotsk Ocean; Paleozoic-Mesozoic,
34 Subduction initiation; Scissor-like closure

35

36 **1. Introduction**

37 Orogenic belt is the one of the best windows to study continental crustal evolution
38 and plate tectonics, therefore, it becomes the frontier and hot realm of the Earth sphere
39 interaction and Earth system science. According to the classical Wilson cycle, an
40 evolution of orogenic belt starts from opening of an oceanic basin, and due to the
41 subduction of oceanic slab, continental blocks approach each other gradually, leading
42 to final collision and formation of orogenic belt. The Mongol-Okhotsk orogenic belt,
43 located in northeastern Asia, recorded the subduction of the Mongol-Okhotsk Ocean
44 (MOO), the collision between the Siberian Craton (SIB) and North China Craton
45 (NCC)-Amuria Block (AMB), as well as the post-orogenic continental uplift
46 (Zonenshain et al., 1990; Zorin et al., 1999; Kelty et al., 2008; Sun et al., 2013; Xu et
47 al., 2013a; Khanchuk et al., 2015; Van der Voo et al., 2015; McDannell et al., 2018;
48 Meng et al., 2020; Sorokin et al., 2020; Yi and Meert., 2020), and it is the last main
49 orogenic belt that constructs the modern tectonic framework of northeastern Asia.
50 Different from a classic collisional orogenic belt, relative rotations of the SIB and NCC-
51 AMB resulted in a scissor-like closure of the MOO from west to east (Zonenshain et
52 al., 1990; Xu et al., 2013a, b; Sun et al., 2013; Wang et al., 2015; Khanchuk et al., 2015;
53 Yang et al., 2015; Gordienko et al., 2019; Sorokin et al., 2020) and the formation of the
54 Mongol orocline (Xiao et al., 2018; Liu et al., 2021; Wang et al., 2022; Li et al., 2022).
55 Therefore, constraining evolution of the MOO in different stages from its initial
56 opening and subduction to final closure will be crucial to decipher the regional tectonics
57 of northeastern Asia. However, due to its long and complex evolutionary history of
58 oceanic subduction and diachronous closure from the Paleozoic-Mesozoic, the tectonic
59 evolution of the MOO is still hotly debated.



60

61 Figure 1. Tectonic framework of northeastern Asia, emphasizing on the Mongol-
 62 Okhotsk suture (modified from Parfenov et al., 2009).

63

64 The Mongol-Okhotsk orogenic belt (original named as fold belt) was firstly
 65 proposed by the Soviet geologist A.E. Fersman in 1926 (Fersman, 1926), suggesting
 66 the final suture of the MOO. It stretches over 3000 km from the Khangay Mountain in
 67 central Mongolia, via northeastern Mongolia and Heilongjiang, to the Uda bay of the
 68 Okhotsk Sea (Figure 1). Due to the lack of geological record, the origin of the MOO is
 69 not well constrained. Zonenshain et al. (1990) proposed a long-term evolution of the
 70 MOO from the Silurian to Jurassic based on geological evidence including Paleozoic-
 71 Mesozoic marine deposits (Kelty et al., 2008; Bussien et al., 2011; Ruppen et al., 2014;
 72 Yang et al., 2015) and subduction related magmatic rocks (Donskaya et al., 2012; 2013;
 73 Sun et al., 2013; Xu et al., 2013a, b; Tang et al., 2014; 2016; Sheldrick et al., 2020)
 74 along the southern margin of the SIB and northern margin of the AMB (constituted by
 75 the Ergun-Kerulen Block, South Mongolia accretionary system, Songliao-Bureya-
 76 Jiamusi-Xingkai Block; Fig 1). For the closure of the MOO, Zonenshain et al. (1990)

77 also suggested a gradual closure of the MOO from west to east based on the west-east
78 younging trend of marine deposits and continental arc magmatism along both sides of
79 the Mongol-Okhotsk suture. This model is supported by geological evidence of
80 multidiscipline and was named as “scissor-like closure” (Natal’in, 1993; Zorin et al.,
81 1999; Sun et al., 2013; Wang et al., 2015; Khanchuk et al., 2015; Yang et al., 2015;
82 Sorokin et al., 2020). However, the timing of the MOO’s closure is still hotly debated.

83 In this paper, by integrating different aspects of geological and geophysical
84 evidence from recent and our own studies, we discussed the initial opening, subduction
85 and final closure of the MOO, especially the most controversial issues and possible
86 breakthrough points. Based on the discussion, we try to constrain the evolution of the
87 MOO and its final closure.

88 **2. Main tectonic units of the Mongol-Okhotsk suture**

89 The over 3000 km Mongol-Okhotsk suture extending from the Khangay Mountain
90 to the Uda Bay shows different evolution histories from west to east, with different rock
91 assemblages, kinematic and metamorphic features for different segments. We divided
92 the Mongol-Okhotsk suture into four segments from west to east (Khangay Mountain,
93 central Mongolia, northeastern Mongolia-Transbaikal and Ergun segments) and
94 compared their rock assemblages, kinematic and metamorphic features in the following.

95 The Khangay Mountain segment represents the westernmost part of the Mongol-
96 Okhotsk suture. Its basement is constituted by the Neoproterozoic-Early Cambrian
97 Bayan-Khongor accretionary complex including ophiolite, arc volcanic rocks, pelagic
98 and shallow marine sediments that was overlain unconformably by the Cambrian-
99 Ordovician Dzag Formation Brachiopods-bearing flysch and carbonate (Figure 2;
100 Gordienko et al., 2019). Age of the Bayan-Khongor ophiolite is 655-636 Ma (Buchan
101 et al., 2001, 2002; Osozawa et al., 2008; Jian et al., 2010), which is overlain by the
102 Cambrian-Ordovician meta-mudstone, meta-sandstone and limestone (Figure 2;
103 Buchan et al., 2001; Badarch et al., 2002). These Neoproterozoic-Early Paleozoic
104 geological units are unconformably overlain by the widespread Devonian-
105 Carboniferous clastic rocks, which represent marginal marine clastic deposits (Figure
106 2; Zonenshain et al., 1990). Detrital zircon dating results from the Devonian-

107 Carboniferous strata reveal a peak age of 359-357 Ma, indicating provenance from the
108 arc magmatic rocks due to bidirectional subduction of the Mongol-Okhotsk oceanic
109 slab (Kelty et al., 2008; Bussien et al., 2011). The Paleozoic marine deposits were
110 unconformably overlain by the Upper Triassic non-marine clastic rocks (Badarch et al.,
111 2002; Zhao et al., under review) and intruded by the Late Triassic granitic rocks (Wang
112 et al., 2022).

113 The central Mongolia segment is located from western Ulaanbaatar to Ondorhaan
114 that is characterized by thick Silurian-Devonian pelagic deposits. Basalt has been
115 identified at the bottom of the Silurian-Devonian sedimentary sequence, which may
116 represent intra-oceanic arc volcanism (Figure 2; Kurihara et al., 2009). The late
117 Silurian-Devonian chert-turbidite are symmetrically distributed on both sides of the
118 suture and overlain by the Carboniferous thick clastic rocks (Minjin et al., 2006). The
119 Silurian-Carboniferous sedimentary sequence can be divided into four formations,
120 namely the Sergelen, Gorkhi, Altanovoo and Orgioch Formations from bottom to top
121 (Minjin et al., 2006). The Sergelen and Gorkhi Formations are mainly composed of
122 chert and turbidite. The Sergelen Formation is weakly metamorphosed without
123 radiolarian or other fossils that can be used for dating, whereas the Gorkhi Formation
124 contains abundant radiolarian that assigned its depositional age of the Late Silurian-
125 Late Devonian (Kashiwagi et al., 2004; Kurihara et al., 2009). The Altanovoo and
126 Orgioch Formations are over 5000m-thick with Early Carboniferous brachiopods and
127 bryozoon (Minjin et al., 2006). Two ophiolitic mélanges have been identified from this
128 segment in the Adaatsag and Khuhu Davaa regions, age of which has been constrained
129 at 325-314 Ma by zircon U-Pb dating (Tomurtogoo et al., 2005; Zhu et al., 2018; 2023a).
130 The Permian and Early Triassic sequences are also marine deposits, indicating that the
131 MOO continued at least until to the Early Triassic in this segment (Zonenshain et al.,
132 1990). Similar to the Khangay Mountain segment, these marine strata were
133 unconformably overlain by the Late Triassic non-marine deposits and intruded by the
134 Late Triassic granitoids (Figure 2).

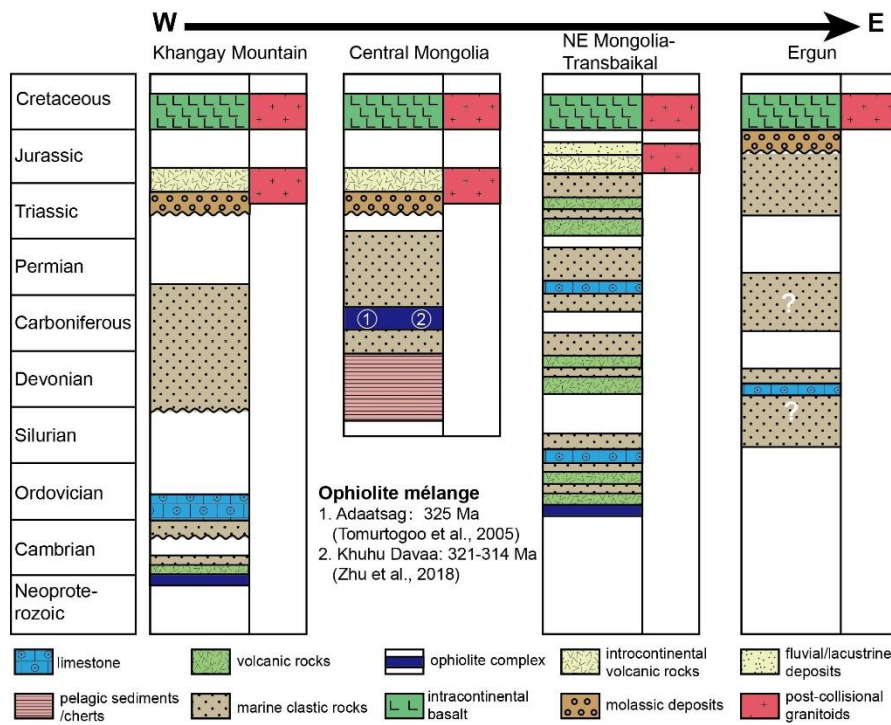
135 The northeastern Mongolia-Transbaikal segment is located in the Choybalsan-
136 Chita region, belonging to the middle part of the Mongol-Okhotsk suture. The basement

137 is constituted by the Early Paleozoic accretionary complex, including the Late
138 Cambrian-Early Ordovician ophiolitic mélange, representing the early stage of the
139 evolution of the MOO (Figure 2; Gordienko et al., 2019). The Early Paleozoic
140 accretionary complex is overlain by the Devonian-Early Carboniferous volcanic-
141 sedimentary sequence (Figure 2), representing the island arc magmatism related to
142 subduction of the Mongol-Okhotsk oceanic slab, such as the Onon island arc in the
143 Mongolia-Russia border (Zorin, 1999). Paleomagnetic results reveal that the Onon
144 island arc was far away from both the SIB and AMB, indicating that the Onon arc
145 should be an intra-oceanic island arc within the MOO (Kuzmin and Kravchinsky, 1996).
146 The arc magmatism ceased before the Late Carboniferous and overlain by Late
147 Carboniferous-Permian shallow marine deposits (Figure 2; Zorin et al., 1995). The
148 second episode of arc magmatism of the Onon arc started from the Late Permian,
149 represented by the Late Permian-Triassic basaltic andesite and andesite. The youngest
150 age obtained from the Onon arc magmatic rocks is ca. 197 Ma, indicating that
151 subduction of the Mongol-Okhotsk oceanic slab continued to the Early Jurassic in this
152 segment (Zorin, 1999). These island arc magmatic rocks were overlain by the Early
153 Jurassic-Early Cretaceous non-marine deposits and intra-continental volcanic rocks,
154 suggesting that the MOO may have closed in the Early-Middle Jurassic in this segment
155 (Figure 2; Arzhannikova et al., 2020; 2022).

156 The Ergun segment is located to the north of the Heilongjiang River. This segment
157 is characterized by the Paleozoic marine sediments and Mesozoic turbidite that mainly
158 distributed in the Oldoy and Gaga-Sagayan Basins on the north margin of the Ergun-
159 Mamyn Block (Kravchinsky et al., 2002a). The Ergun-Mamyn Block, considered as the
160 northeastern part of the AMB, is composed of the Late Archean-Neoproterozoic
161 basement and Neoproterozoic metamorphosed sedimentary sequence and Cambrian
162 deformed sediments (Tang et al., 2013; Khanchuk et al., 2015; Sorokin et al., 2016).
163 The Ediacaran-Early Ordovician arc magmatic rocks have been identified from the
164 Ergun-Mamyn Block, which may represent continental arc magmatism during the
165 evolution of the Paleo-Asian Ocean (Sorokin et al., 2017). Magmatic rocks are scarce
166 within the suture zone. The Pikan magmatic complex, containing mainly meta-gabbro

167 and diorite, was identified from the northern margin of the Ergun Block as tectonic lens
168 (Sorokin et al., 2007; 2020). Zircon U-Pb dating constrains the emplacement of the
169 Pikan magmatic complex in the Middle Ordovician-Early Devonian (468-415 Ma),
170 which was interpreted as continental marginal arc magmatic rocks that were drawn into
171 the suture zone during the evolution of the MOO (Sorokin et al., 2007; 2020). Within
172 the Mongol-Okhotsk suture, the Silurian-Jurassic marine sediments were well
173 preserved (Figure 2). The Silurian strata are composed of metamorphosed sandstone,
174 siltstone and conglomerate. The Devonian strata consist of metamorphosed sandstone,
175 siltstone, limestone and chert with tuff interlayers. The Carboniferous sequence is
176 composed of metamorphosed sandstone, siltstone and limestone. The Lower Permian
177 strata consist of mudstone, greenschist and meta-sandstone with lens of chert and
178 limestone (Figure 2; Turbin, 1994; Serezhnikov and Volkova, 2007). Ages of the
179 Devonian-Permian strata were determined by fossils within the strata including coral,
180 brachiopods and bryozoon. However, as these strata suffered from severe
181 metamorphism and deformation, these fossils are not well preserved, resulting in
182 questionable age assignment of these strata. Recent detrital zircon dating results from
183 the Devonian Tungala, Dugda and Tangomen Formations in the Tukuringra terrane
184 revealed the youngest peak ages of 207 Ma, 181 Ma and 189 Ma, respectively,
185 indicating that they were Jurassic sediments (Sorokin et al., 2020). Meanwhile, the
186 youngest peak ages for the Carboniferous Dzheskogon and Nekter Formations and
187 lower Permian Bochagor Formation were obtained at 244 Ma, 202 Ma and 255 Ma,
188 respectively, suggesting that they were deposited in the Triassic-Jurassic rather than the
189 Carboniferous-Permian (Sorokin et al., 2020). Therefore, most previously considered
190 Paleozoic strata may be deposited in the Triassic-Jurassic and the existence of Paleozoic
191 marine strata is questionable that need further evidence. Detrital zircon dating results
192 also indicate that marine deposits in the Ergun segment continued at least to the Early
193 Jurassic, supporting previous consideration that there were Early Jurassic marine
194 deposition in this region (Parfenov et al., 2001). The transition from marine to non-
195 marine sedimentary environment, occurred in the Middle Jurassic and represented by
196 the Middle-Late Jurassic coal-bearing continental deposits in the Amur, Zeya and Mohe

197 Basins, suggests the closure of the MOO and formation of the Mongol-Okhotsk
 198 orogenic belt (Figure 3; He et al., 2015; Smirnova et al., 2017; Duan et al., 2021).



199

200 Figure 2. Strata columns of different segments of the Mongol-Okhotsk suture.
 201 (synthesized from 1:500,000 geological map of Mongolia and data from Badarch et al.,
 202 2002; Kurihara et al., 2009; Gordienko et al., 2019; Chen et al., 2022). Chronological
 203 data of ophiolitic mélange are from Tomurgogoo et al., 2005 and Zhu et al., 2018.

204

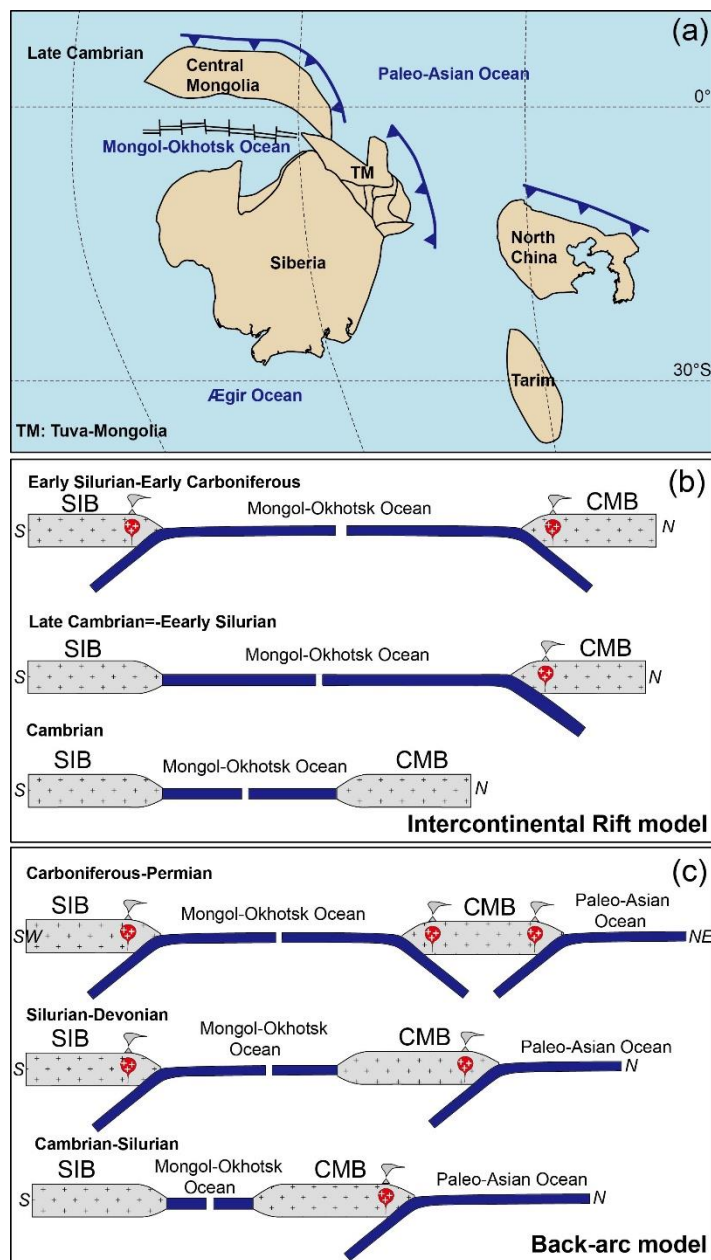
205 3. Origin and subduction of the Mongol-Okhotsk Ocean

206 Due to the lack of geological evidence, the origin of the MOO has not been well
 207 constrained. Nevertheless, based on the Ordovician-Silurian slices of oceanic slab
 208 identified in central and northern Mongolia, the opening of the MOO has been
 209 connected with the evolution of the Paleo-Asian Ocean (Figure 3a; Zonenshain et al.,
 210 1990; Cocks and Torsvik, 2007; Ruppen et al., 2014). Gordienko et al. (2019) proposed
 211 a rift-extension model that the MOO originated from extension of the Orkhon-Kharagol
 212 basin between the Central Mongolian and Muya-Stanovoi Blocks (Figure 3b). Another
 213 model suggests that subduction of the Paleo-Asian oceanic slab beneath the SIB in the
 214 Early Paleozoic caused back-arc extension that evolved into the MOO (Figure 3c;
 215 Badarch et al., 2002; Bussien et al., 2011; Cocks and Torsvik, 2007). Both two models

216 resulted in the rifting and drifting of the Central Mongolian Block (constituting the
217 AMB since the Late Paleozoic) from the SIB with the opening of the MOO (Figure 3a;
218 Torsvik and Cocks, 2016). The similar rifting and drifting processes also occurred for
219 the Western Mongolian Blocks (constituted by the Tuva-Mongolia, Zavkhan, Baydrag
220 and Tarvagatay Blocks). The Western Mongolian Blocks accreted to the margin of the
221 SIB during the Neoproterozoic-Ordovician (Badarch et al., 2002). After short-term
222 coevolution, the Western Mongolian Blocks rifted from the SIB in the Silurian and
223 drifted southward, revealed by paleomagnetic results (Bold et al., 2016; Kilian et al.,
224 2016). However, as no Early Paleozoic paleomagnetic result has ever been reported
225 from the AMB, it is still debatable whether the AMB was rifted from the SIB in the
226 Early Paleozoic or the oceanic basin between the SIB and AMB existed before the Early
227 Paleozoic that was named as the MOO since the Early Paleozoic. For example, both
228 Zorin (1999) and Li (2006) considered that the MOO was a gigantic bay of the Paleo-
229 Pacific Ocean between the SIB and AMB.

230 The subduction of the Mongol-Okhotsk oceanic slab initiated in the Silurian. Calc-
231 alkaline granotoids and accretionary complex identified along the southern margin of
232 the SIB are the direct evidence for subduction of the Mongol-Okhotsk oceanic
233 subduction (Zorin, 1999; Donskaya et al., 2013; Ruppen et al., 2014). Meanwhile,
234 detrital zircon dating results obtained from the Devonian-Carboniferous strata to the
235 north of the suture display Silurian-Devonian age peaks (Ruppen et al., 2014),
236 indicating arc magmatism related to the subduction of the Mongol-Okhotsk oceanic
237 slab beneath the southern margin (recent coordinates) of the SIB. The widely distributed
238 Devonian-Carboniferous turbidites in the western and central parts of the Mongol-
239 Okhotsk suture represent trench sediments along Andean-type continental margin
240 (Zorin, 1999). The Silurian-Devonian magmatic rocks have also been identified from
241 the southern side of the suture, but it is still controversial whether they can represent
242 subduction-related magmatism or not. For example, the Late Silurian bimodal volcanic
243 rocks identified on the Ereendavaa Block (northeastern part of the AMB) was
244 interpreted as post-collisional magmatism following collision between the Ereendavaa
245 Block and the Idermeg Block (Narantsetseg et al., 2019). The Late Devonian A-type

246 granite reported from the Ergun Block resulted from the northwestward subduction of
 247 the Heihe-Nenjiang oceanic slab beneath the Ergun Block (Li et al., 2017a). Meanwhile,
 248 detrital zircon dating results show that different peak ages from the Silurian-Middle



249
 250 Figure 3. Models of opening of the Mongol-Okhotsk Ocean. (a) Paleogeography map
 251 of the Siberian Craton and surrounding cratons in the Late Cambrian (modified from
 252 Torsvik and Cock, 2016); (b) Intercontinental rift model (modified from Gordienko et
 253 al., 2019); (c) Back-arc extension model (modified from Bussien et al., 2011). SIB:
 254 Siberian Craton; CMB: Central Mongolian Block.

255

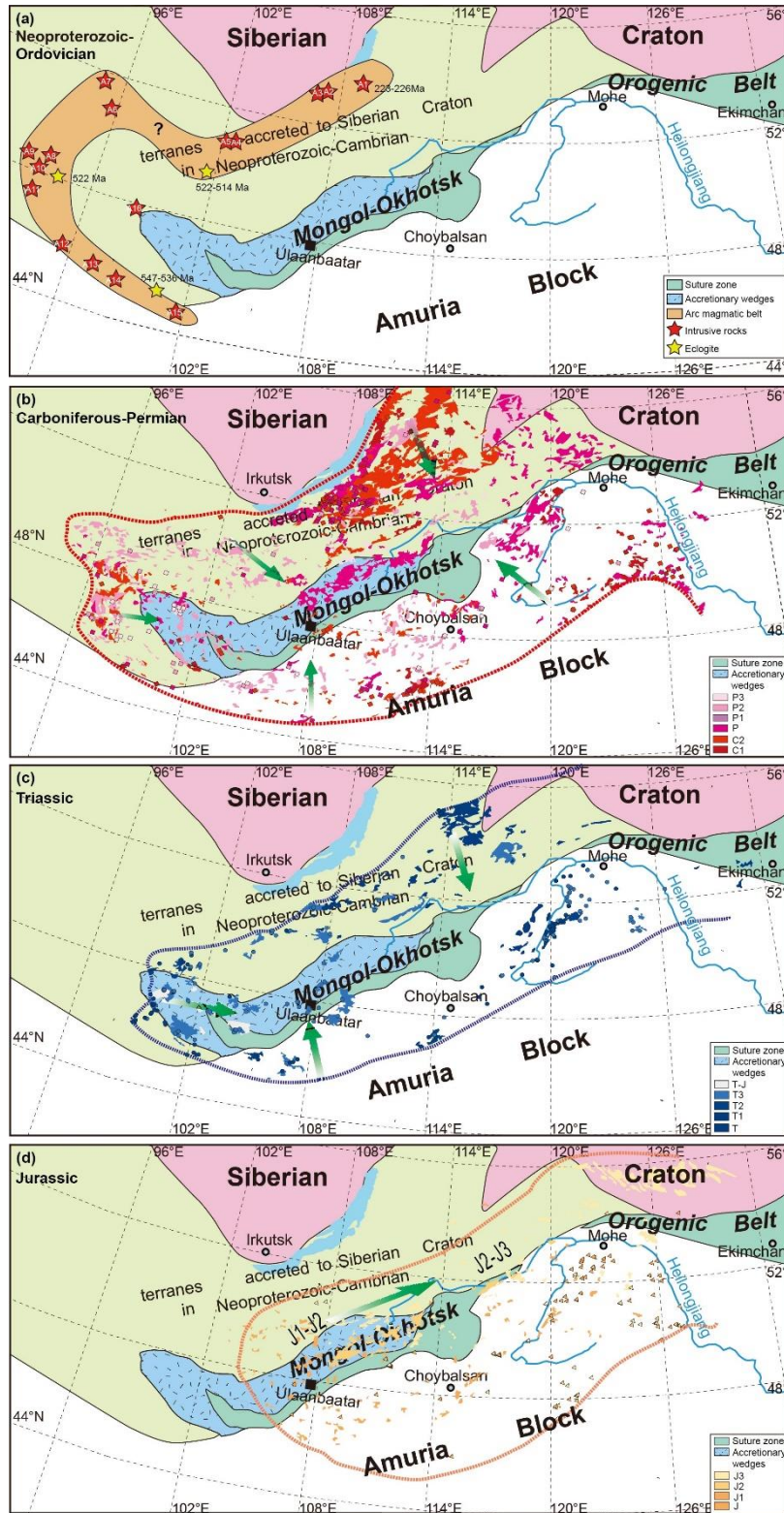
256 Devonian obtained from the northern side of the suture (Ruppen et al., 2014). However,
257 strata in the southern side of the suture display no Silurian-Middle Devonian age peak
258 (Bussien et al., 2011). The different detrital zircon age distribution patterns may
259 consequently suggest that there was no southward subduction of the Mongol-Okhotsk
260 oceanic slab beneath the northern margin of the AMB during the Silurian-Middle
261 Devonian. Detrital zircon dating results obtained from the Carboniferous strata in the
262 western segment of the suture reveal a significant age peak at about 351 Ma and some
263 Late Devonian zircon ages (Kelty et al., 2008), indicating that the southward subduction
264 of the MOO may have started in the Late Devonian and reached its climax in the Early
265 Carboniferous. Recent studies show that subduction of the MOO may have started since
266 the Cambrian-Ordovician. A new Cambrian-Ordovician Ikh-Mongol magmatic belt has
267 recently been identified around the Mongol-Okhotsk suture with coeval subduction-
268 related high-pressure eclogite (Figure 4a; Janoušek et al., 2018; Zhu et al., 2023b). But
269 how this magmatic belt was formed is not clear. Although it was considered as the result
270 of the subduction of the Paleo-Asian Ocean beneath the Tuva-Mongolia Block
271 (Janoušek et al., 2018), due to their distribution along the Mongol-Okhotsk suture, they
272 may also represent the Cambrian-Ordovician subduction of the MOO. More studies are
273 need to decipher the tectonic origin of this magmatic belt. Meanwhile, two Ordovician
274 high-K granites have recently been identified with zircon U-Pb age of 469 ± 3 Ma and
275 440 ± 3 Ma (Ling et al., 2021). Both granitic bodies show A₂-type geochemical
276 characteristics, which was interpreted as the result from slab roll-back during the
277 subduction of the MOO in the Middle Ordovician (Ling et al., 2021). Based on the
278 study of the Late Carboniferous Adaatsag ophiolite, Zhu et al. (2023a) found that it has
279 similar rock assemblage with the Izu-Bonin-Mariana forearc magmatic rocks, therefore,
280 they proposed that the southward subduction of the MOO may initiated from the Late
281 Carboniferous. However, this subduction initiation timing is not consistent with the
282 Early Carboniferous age peak of magmatic rocks along the suture (Kelty et al., 2008).

283 The bidirectional subduction of the Mongol-Okhotsk oceanic slab resulted in
284 abundant arc magmatic rocks along both continental margins of the SIB and AMB
285 (Figure 4b; Donskaya et al., 2013; Zhao et al., 2017; Wang et al., 2022). To the north of

286 the suture, arc magmatic rocks contain mainly of granite, granodiorite, monzogranite,
287 syenite and mafic rocks, showing typical continental margin arc magmatic geochemical
288 affinity (Donskaya et al., 2013). To the south of the suture, arc magmatic rocks are
289 mainly composed of I-type calc-alkaline to high-K calc-alkaline granite, monzogranite
290 and syenogranite (Zhao et al., 2017; Li et al., 2018; Sorokin et al., 2021). Detrital zircon
291 dating results obtained from Carboniferous strata within and along both sides of the
292 suture show a prominent Early Carboniferous age peak, supporting the widely
293 distributed subduction-related Early Carboniferous arc magmatism (Figure 5; Kelty et
294 al., 2008; Bussien et al., 2011). Meanwhile, detrital zircon dating results reveal three
295 age peaks of Early Carboniferous (351-344 Ma), Late Permian (257-254 Ma) and Late
296 Triassic-Early Jurassic (207-192 Ma) for the arc magmatism related to the Mongol-
297 Okhotsk oceanic subduction (Figure 5; Kelty et al., 2008; Sorokin et al., 2020; Chen et
298 al., 2022), indicating pulse magmatic events that may be related to changes of angle
299 and velocity of the subducted slab. By compilation of magmatic rocks along both sides
300 of the suture, Wang et al. (2022) found that ages of magmatic rocks show outside to
301 inside younging and west to east younging trends (Figure 4b-d). The Carboniferous-
302 Early Triassic magmatic rocks have been identified around the whole suture (Tang et
303 al., 2014; 2016; Zeng et al., 2014; Ji et al., 2018; Fu et al., 2021; Sorokin et al., 2021;
304 Wang et al., 2022; Ovchinnikov et al., 2023), whereas the Jurassic magmatic rocks are
305 only distributed in the central and eastern segments of the suture (Figure 4c,d; Xu et al.,
306 2013a; Sun et al., 2013; Wang et al., 2015; Sheldrick et al., 2020), indicating that the
307 subduction in the western segment may have ceased at the Late Triassic.

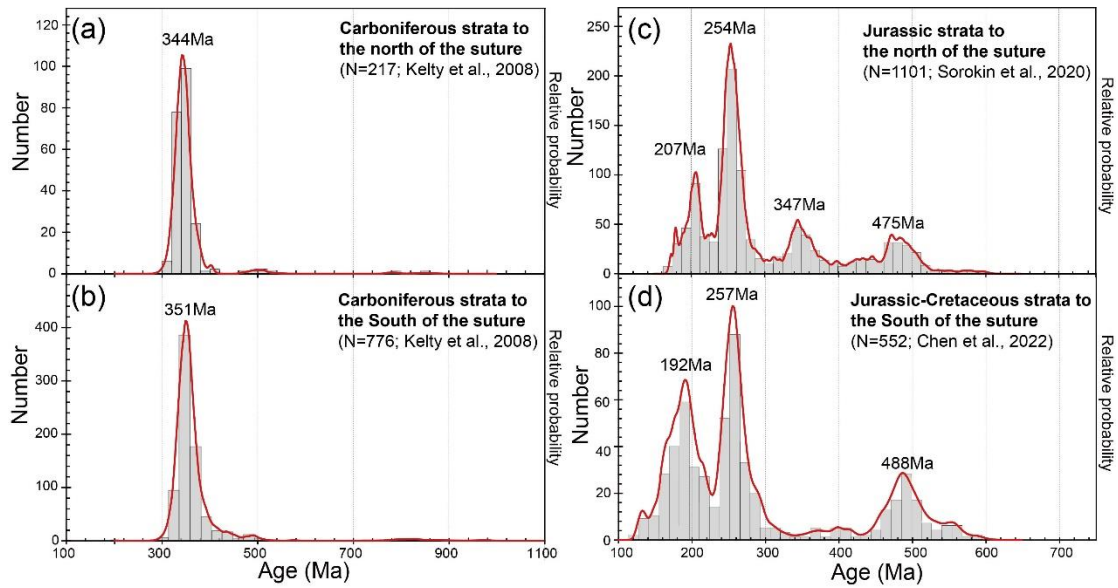
308 Magmatic rocks along the southern margin of the SIB and northern margin of the
309 AMB reveal a bidirectional subduction of the MOO. However, seismic topography
310 results only show high velocity anomaly beneath the SIB, without high velocity
311 anomaly beneath the AMB (Van der Voo et al., 1999; van der Meer et al., 2018), arguing
312 for a solo northward rather than bidirectional subduction of the MOO (Van der Voo et
313 al., 1999). However, the geodynamic modeling shows that due to eastward movement
314 and rotation of the Eurasia continent, if there was southward subduction, the subducted
315 oceanic slab could be preserved beneath the SIB (Fritzell et al., 2016). Therefore, the

316 absence of high velocity anomaly beneath the AMB cannot be considered as the
 317 evidence arguing against the southward subduction of the MOO beneath the AMB.



318
 319 Figure 4. Distribution of magmatic rocks in different ages around the Mongol-Okhotsk
 320 suture. (a) Ediacara-Ordovician (modified from Zhu et al., 2023b); (b) Carboniferous-

321 Permian (modified from Wang et al., 2022); (c) Triassic (modified from Wang et al.,
322 2022); (d) Jurassic (modified from Wang et al., 2022).



323
324 Figure 5. Detrital zircon distribution patterns of Carboniferous (a, b) and Jurassic-
325 Cretaceous (c, d) strata from both sides of the Mongol-Okhotsk suture, showing
326 similar Earliest Carboniferous, Late Permian and Late Triassic-Early Jurassic age
327 peaks from both sides of the Mongol-Okhotsk suture. Detrital zircon U-Pb age data
328 are from Kelty et al., 2008; Sorokin et al., 2020 and Chen et al., 2022.

329

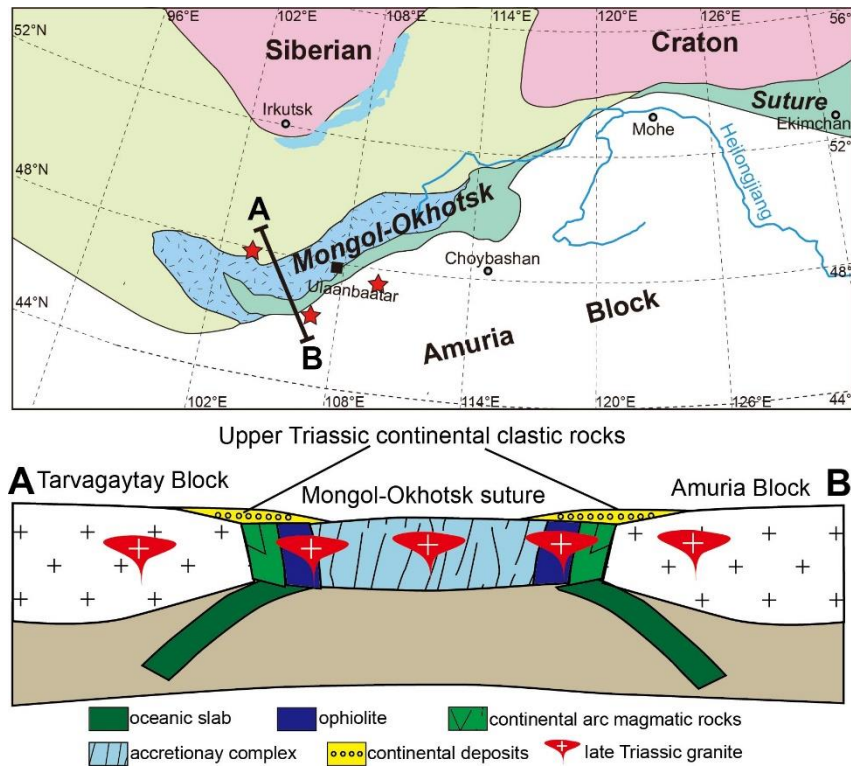
330 4. Closure of the Mongol-Okhotsk Ocean

331 The style and timing of closure are the most controversial problems for the
332 evolution of the MOO. Geological evidence argues for a west to east scissor-like closure
333 of the MOO (Zonenshain et al., 1990; Zorin, 1999; Xu et al., 2013a; Gordienko et al.,
334 2019; Sorokin et al., 2020; Arzhannikova et al., 2020; Wang et al., 2022). For example,
335 both transition timing from marine to non-marine sediments and ages of magmatic
336 rocks show an eastward younging trend along the suture (Zonenshain et al., 1990; Wang
337 et al., 2022). The scissor-like closure is also supported by paleomagnetic result. By
338 compilation of paleomagnetic data from blocks in eastern Asia, Zhao et al. (1996)
339 proposed that the western segment of the MOO was closed in the Late Permian-Triassic,
340 whereas the eastern segment was closed in the Late Jurassic-Early Cretaceous. On the
341 contrary, both Enkin et al. (1992) and Van der Voo et al. (2015) considered that the

342 MOO was simultaneously closed in the Late Jurassic-Early Cretaceous. During the
343 Triassic-Jurassic, the SIB experienced $\sim 45^\circ$ clockwise rotation and moved southward,
344 and the NCC-AMB rotated $\sim 90^\circ$ counterclockwise and moved northward (Van der Voo
345 et al., 2015). In this model, the relative rotations of the SIB and NCC-AMB caused
346 narrowing of the MOO in a scissor-like way, resulting in the similar width of the MOO
347 from west to east in the Late Jurassic and closure of the MOO in the Late Jurassic-Early
348 Cretaceous. Recent sedimentological and detrital zircon dating studies on the western
349 Baikal region (central segment of the MOO) and the Dzhagda region (eastern segment
350 of the MOO) argue for that the central and eastern segments of the MOO should have
351 been closed in the Early-Middle Jurassic boundary (Arzhannikova et al., 2020; Sorokin
352 et al., 2020). However, remnant-oceanic basin still existed in the eastern Baikal region
353 that was closed in the Middle to Late Jurassic boundary, based on which Arzhannikova
354 et al. (2022) proposed that the closure of the MOO may not be in the scissor-like way
355 and each segment of the MOO evolved independently. The main reason for this
356 controversy is that the timings for the initial and final closure of the MOO are not well
357 constrained.

358 **4.1 Timing of initial closure of the MOO in its western segment**

359 Zonenshain et al. (1990) proposed that the initial closure of the MOO in its western
360 segment occurred in the Late Triassic-Early Jurassic based on the transition age from
361 marine to non-marine deposits and ages of magmatic rocks along the Mongol-Okhotsk
362 suture. This viewpoint is supported by the regional unconformity identified between
363 the Upper Triassic clastic deposits and underlying geological units (Badarch et al.,
364 2002). Meanwhile, the Late Triassic alkaline magmatic rocks were identified from the
365 western segment of the Mongol-Okhotsk suture, emplaced in an extensional setting,
366 arguing for a Late Triassic closure of the MOO in its western segments (Donskaya et
367 al., 2013). Furthermore, the Late Triassic granites intruded into the Mongol-Okhotsk
368 suture as stitching plutons and the Jurassic arc magmatism did not exist anymore along
369 the western segment of the Mongol-Okhotsk suture (Figure 6; Wang et al., 2022). Based
370 on these evidence, a Late Triassic closure of the MOO in its western segment was
371 proposed, followed by scissor-like closure of the MOO (Wang et al., 2022).



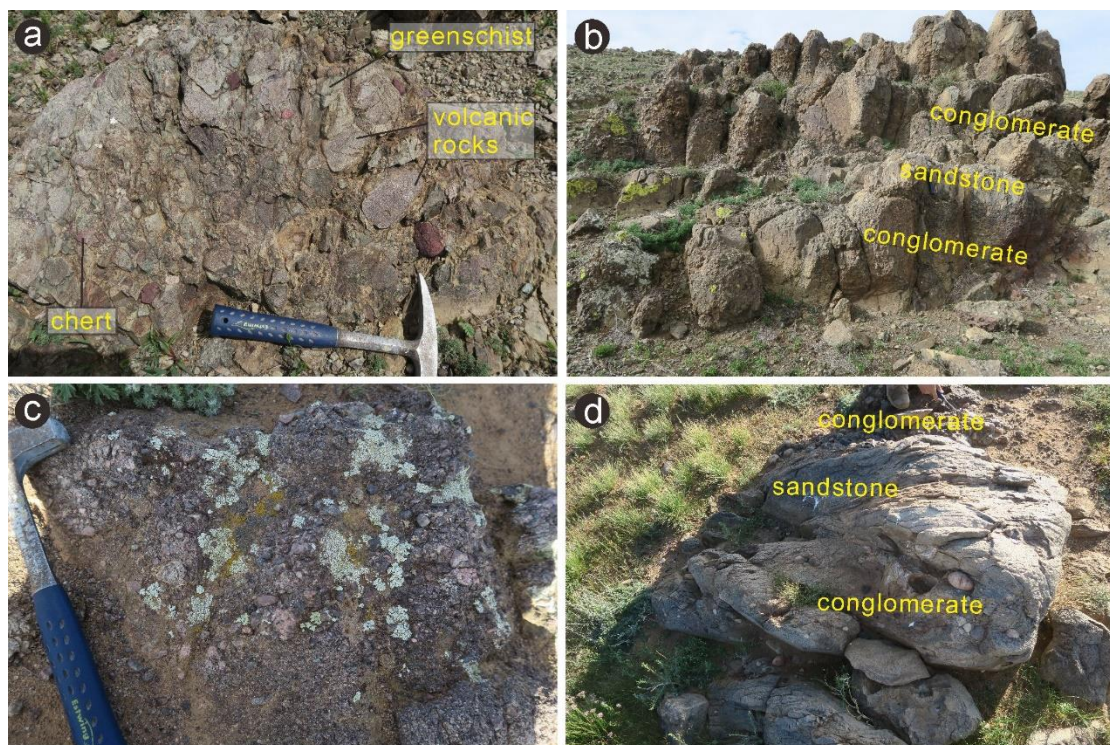
372

373 Figure 6. Cross-section across-cut the western segment of the Mongol-Okhotsk suture
 374 with location marking in the upper map. Late Triassic granites intruded into the suture
 375 zone and Tarvagatay Block and Amuria Block on both sides of the suture. The suture
 376 zone is unconformably overlain by the Upper Triassic continental clastic rocks.
 377 Magmatic and sedimentary evidence indicates that the western segment of the MOO
 378 should have been closed in the Late Triassic. Red stars represent locations of the
 379 measured Upper Triassic strata and paleomagnetic sampling.

380

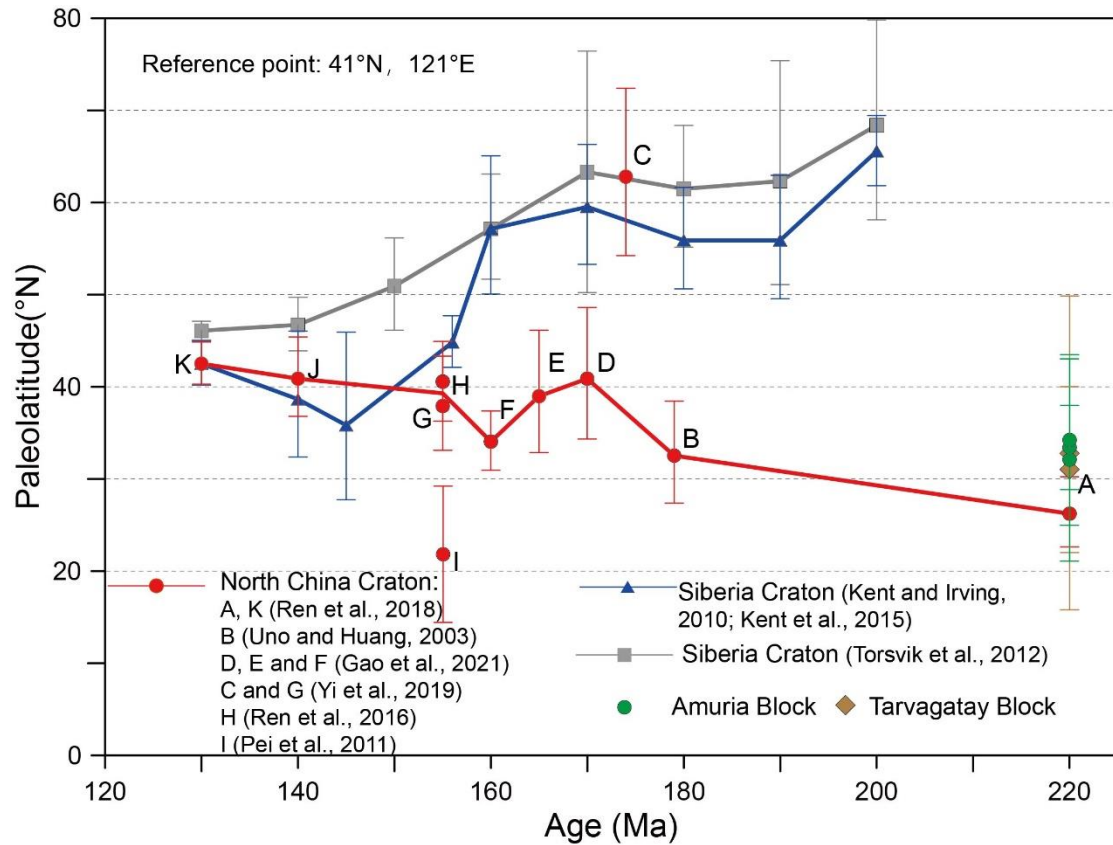
381 Concerning the initial closure of the MOO, different models have been proposed
 382 by paleomagnetic studies. By compilation of paleomagnetic data from the SIB and NCC,
 383 [Zhao et al. \(1996\)](#) considered that the western segment of the MOO should have been
 384 closed during the Permian-Triassic. On the contrary, [Van der Voo et al. \(2015\)](#) proposed
 385 a Late Jurassic-Early Cretaceous simultaneous closure of the whole MOO from west to
 386 east. The southern margin of the SIB aligned in the N-S direction in the Permian and
 387 the Western Mongolian Blocks along the southwestern margin of the SIB ([Figure 1](#))
 388 should collide with the AMB firstly during the clockwise rotation of the SIB that led to
 389 initial closure of the MOO. New paleomagnetic data obtained in the last decade show

390 that the Western Mongolian Blocks accreted to the southwestern margin of the SIB
391 during the Neoproterozoic-Cambrian (Bold et al., 2016). After a short-time coevolution,
392 the Western Mongolian Blocks rifted from the SIB in the Silurian and drifted southward
393 to a middle- to low-latitude since then (Bold et al., 2016; Kilian et al., 2016) until at
394 least to the Carboniferous (Ren et al., 2021). Due to the lack of Permian-Middle Triassic
395 paleomagnetic result for the Western Mongolian Blocks, relative positions of the
396 Western Mongolian Blocks and the SIB during this period cannot be confined. However,
397 considering that the SIB was located at high latitude during the Permian-Middle
398 Triassic (e.g., the paleolatitude of the northern SIB was $\sim 70\text{-}60^\circ$ N during the Permian-
399 Late Triassic; Walderhaug et al., 2005; Torsvik et al., 2012), the initial closure of the
400 MOO in its western segment should be caused by the collision between the Western
401 Mongolian Blocks and the AMB. Pruner (1992) firstly reported a Triassic paleolatitude
402 of $32.8 \pm 16.8^\circ$ N from the Tarvagatay Block (a part of the Western Mongolian Blocks)
403 to the north of the Mongol-Okhotsk suture. Although this paleolatitude yielded a big
404 uncertainty, it is consistent with coeval paleolatitude of the NCC-AMB (Wu et al., 1990;
405 Yang et al., 1991; Ma et al., 1993).



406
407 Figure 7. Photos of field outcrops of the Upper Triassic continental clastic rocks from
408 the western segment of the Mongol-Okhotsk suture. Basal conglomerate (a) and

409 interbedded conglomerate and sandstone (b) from northern side of the suture, with
 410 pebbles and cobbles of volcanic rocks, greenschist, chert, etc. Basal conglomerate (c)
 411 and interbedded conglomerate and sandstone (d) from the southern side of the suture.
 412



413
 414 Figure 8. Paleolatitude versus time plot with the Late Triassic-Early Cretaceous
 415 paleomagnetic data of the NCC, SIB, AMB and the Tarvagatay Block.
 416 Paleolatitude data of the NCC are from Uno and Huang, 2003; Pei et al., 2011;
 417 Ren et al., 2016; 2018 and Gao et al., 2021. Paleolatitude data of the SIB are from
 418 Kent and Irving, 2010 and Kent et al., 2015. Paleolatitude data of the NCC and
 419 SIB are calculated with reference point of 41°N, 121°E. Paleolatitude data of the
 420 AMB and the Tarvagatay Block are from Pruner, 1992; Zhao et al., 2023 and Zhao
 421 et al., under review. Paleolatitude data of the AMB and the Tarvagatay Block are
 422 calculated with individual sampling location.

423
 424 To test this latitudinal consistency, we performed sedimentological and
 425 paleomagnetic studies on the Upper Triassic strata from both sides of the western

426 segment of the Mongol-Okhotsk suture zone. The Upper Triassic strata from both sides
427 of the suture show similar terrestrial deposits (Figure 6), with thick-bedded
428 conglomerate at the bottom containing pebbles and cobbles of chert, greenschist,
429 volcanic rocks etc. (Figure 7a, c), interbedded conglomerate-sandstone in the middle
430 (Figure 7b, d), and thick-bedded sandstone in the upper part. The rock assemblages,
431 combining with abundant plant fossils discovered from sandstone layers, indicate that
432 the Late Triassic sedimentary sequence represents foreland basin deposits after the
433 closure of the western segment of the MOO (Figure 6; Zhao et al., under review). Our
434 paleomagnetic studies on the Upper Triassic strata show paleolatitudes of $31.1^{\circ} \pm 9.0^{\circ}\text{N}$
435 for the Tarvagatay Block, $32.1^{\circ} \pm 10.6^{\circ}\text{N} \sim 34.2^{\circ} \pm 9.2^{\circ}\text{N}$ for the northern margin of the
436 AMB, and $33.3^{\circ} \pm 4.6^{\circ}\text{N}$ for the southern margin of the AMB (Figure 8; Zhao et al.,
437 2023). The consistent paleolatitudes for the Tarvagatay Block and the AMB indicate that
438 the MOO may have been closed in the Late Triassic.

439 By integrating sedimentological, magmatic, paleontological and paleomagnetic
440 evidence, we propose that the Western Mongolian Blocks have collided with the NCC-
441 AMB in the Late Triassic, and the initial closure of the western segment of the MOO
442 occurred in the Late Triassic (Figure 9b).

443 **4.2 Timing of final closure of the MOO in its eastern segment**

444 Multi-disciplinary studies have been performed on the final closure of the MOO
445 in its eastern segment. However, due to different methodologies and materials in focus,
446 timing of final closure of the MOO is still hotly debated, with three main viewpoints at
447 the Early-Middle Jurassic (Zorin, 1999; Sorokin et al., 2020; Yi and Meert, 2019), latest
448 Middle Jurassic (Zonenshain et al., 1990; Zhang, 2011; Li et al., 2015; Sun et al., 2013;
449 Xu et al., 2013a; Wang et al., 2015; Li et al., 2018), and Late Jurassic-Early Cretaceous
450 (Kravchinsky et al., 2002a, b; Cogné et al., 2005; Pei et al., 2011; Van der Voo et al.,
451 2015; Yang et al., 2015; Ren et al., 2018).

452 Based on detailed structural kinematic and magmatic studies, Russian geologists
453 proposed that the SIB and NCC-AMB should have collided in the Early-Middle
454 Jurassic (Zorin, 1999). Recent detrital zircon geochronological studies on the meta-
455 sediments from terranes to the north of the Heilongjiang River revealed that their

456 provenance contains materials in the northern AMB (Sorokin et al., 2020). Meanwhile,
457 the absence of detrital zircon younger than 171 Ma implies that the final closure of the
458 MOO could have taken place at the boundary of the Early and Middle Jurassic as a
459 result of the collision between the SIB and NCC-AMB (Zaika et al., 2018; Sorokin et
460 al., 2020). Recent paleomagnetic study on the Lower-Middle Jurassic Nandaling
461 Formation (~174 Ma) in the northern margin of NCC shows a paleolatitude of $61.7^\circ \pm$
462 9.1°N for the NCC, which is consistent with that of the SIB (Figure 8), therefore
463 suggests that the MOO should have been closed at the Early and Middle Jurassic
464 boundary (Yi and Meert, 2020).

465 According to the eastward younging trend of sedimentary and magmatic rocks on
466 both sides of the Mongol-Okhotsk suture, Zonenshain et al. (1990) proposed that the
467 main part of the MOO should have been closed in the Middle Jurassic, with only ~300
468 km width residual oceanic basin left in the easternmost segment. A same conclusion has
469 also been reached based on the ages of kinematic deformation and magmatic rocks
470 (Natal'in, 1993). Kinematic studies on the Jurassic strata in the Heilongjiang Basin
471 revealed a Late Jurassic top-to-the-south thrust, caused by regional compression related
472 to the collision between the SIB and NCC-AMB, suggesting a Middle Jurassic closure
473 of the MOO (Zhang, 2011). Magmatic rocks in the Ergun and Xing'an Blocks show a
474 transition from Late Triassic-Early Jurassic calc-alkaline magmatism to Late Jurassic-
475 Early Cretaceous A-type magmatism with a Middle Jurassic magmatic lull, suggesting
476 that the closure of the MOO should occur in the Middle Jurassic (Sun et al., 2013).
477 Meanwhile, Li et al. (2015) identified a Middle Jurassic (~168 Ma) muscovite granite
478 in NE China, the primary magma of which was derived from partial melting of a
479 juvenile thickened lower crust resulted from closure of the MOO, therefore indicating
480 a Middle Jurassic closure of the MOO. Moreover, the Late Jurassic-Early Cretaceous
481 magmatic rocks emplaced in extensional tectonic setting are widespread distributed in
482 NE Mongolia and western Great Xing'an Range of NE China (Sun et al., 2013; Li et
483 al., 2018; Tang et al., 2018). However, whether these magmatic rocks emplaced in a
484 post-orogenic extension after the closure of the MOO or back-arc extension related to
485 the subduction of the Paleo-Pacific oceanic slab is still controversial. The key to solve

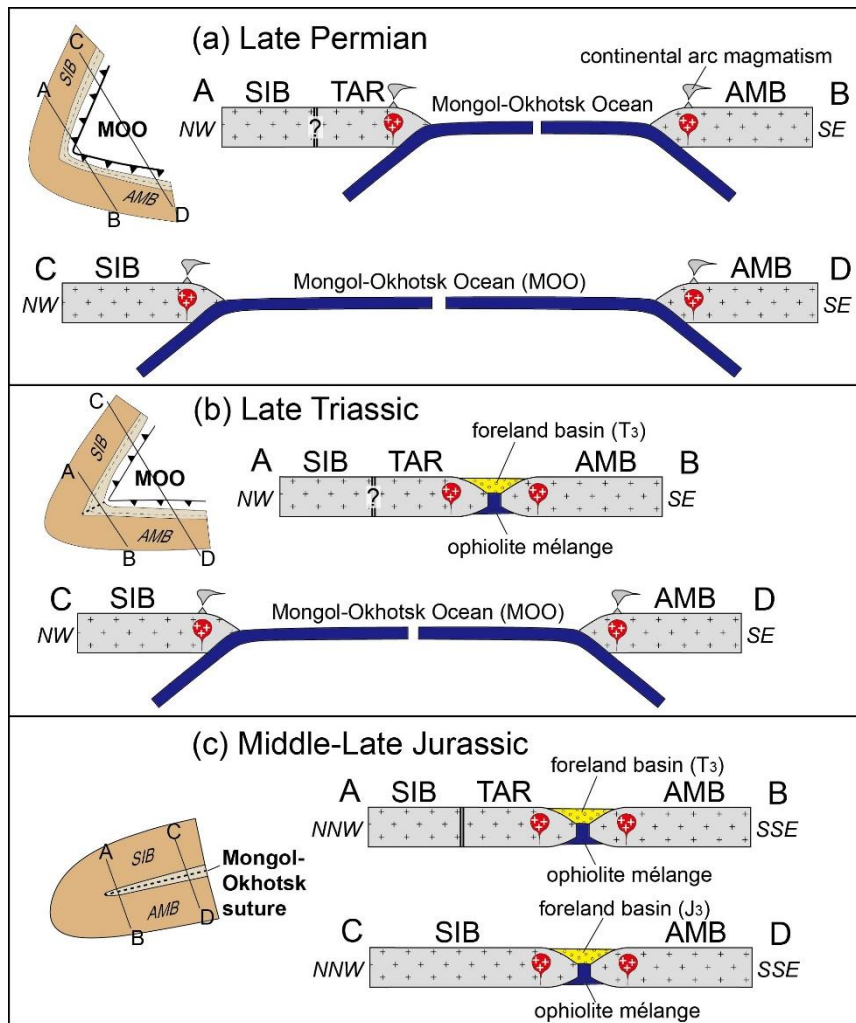
486 this controversy is constraining regions of influence of both two tectonic regimes. [Li et](#)
487 [al. \(2017b\)](#) identified Middle-Late Triassic high-Mg adakitic andesites along the
488 southern margin of the Xing'an Block, and concluded that the Mongol–Okhotsk
489 tectonic regime extended at least as far as the eastern margin of the Xing'an Block.
490 Meanwhile, the Late Jurassic and early Early Cretaceous magmatic rocks are mainly
491 distributed in the Great Xing'an Range and to its west showing a southward migration,
492 while coeval magmatism is scarce in the Lesser Xing'an–Zhangguangcai Ranges and
493 eastern Heilongjiang–Jilin Provinces ([Xu et al., 2013a](#)). Therefore, these Late Jurassic
494 and early Early Cretaceous magmatic rocks should be formed in a post-collisional
495 tectonic setting after the closure of the MOO in the Middle Jurassic, rather than induced
496 by the Paleo-Pacific subduction ([Sun et al., 2013](#); [Xu et al., 2013a](#); [Tang et al., 2015](#);
497 [Wang et al., 2015](#); [Li et al., 2018](#); [Tang et al., 2018](#)).

498 Although paleomagnetic results from the NCC-AMB are inconsistent, most
499 available data indicate the existence of a wide oceanic basin between the SIB and the
500 NCC-AMB. For example, Late Jurassic paleomagnetic data obtained from northern
501 margin of the AMB and southern margin of the SIB show a 1700–2700 km distance
502 between the SIB and AMB ([Kravchinsky et al., 2002a, b](#); [Cogné et al., 2005](#)). Two ca.
503 155 Ma paleomagnetic poles were reported from the northeastern Inner Mongolia and
504 southern Mongolia of the AMB, indicating a paleolatitudinal difference of 10°–15° for
505 the SIB and AMB ([Zhao et al., 1990](#); [Ren et al., 2018](#)). However, paleomagnetic studies
506 on the Late Jurassic Tiaojishan volcanic rocks display different results. [Pei et al. \(2011\)](#)
507 reported a paleomagnetic pole for the Tiaojishan volcanic rocks at 59.9°N/240.3°E,
508 with $A_{95}=6.8^\circ$, constraining a ~3000 km width of the MOO at ca. 155 Ma ([Figure 8](#)).
509 On the contrary, a new paleomagnetic study on the Tiaojishan volcanic rocks yielded a
510 paleomagnetic pole at 69.6°N/203.0°E ($A_{95}=5.6^\circ$), indicating a ~1600 km width of the
511 MOO at ca. 155 Ma ([Figure 8](#); [Ren et al., 2016](#)). The Early Cretaceous paleomagnetic
512 data obtained from southern SIB ([Cogné et al., 2005](#); [Metelkin et al., 2010](#)) and AMB
513 ([Pruner, 1987](#); [Halim et al., 1998](#); [Hankard et al., 2005](#); [Ren et al., 2018](#)) show
514 consistent paleomagnetic pole and paleolatitude, indicating that the MOO should have
515 been closed in the Early Cretaceous. Meanwhile, the apparent polar wander paths

516 (APWPs) of both the NCC and the SIB are overlapped in the Early Cretaceous, also
517 supporting that final closure of the MOO in the early stage of the Early Cretaceous ([Van
518 der Voo et al., 2015](#)). This viewpoint is supported by sedimentary and magmatic
519 evidence. [Yang et al. \(2015\)](#) identified a Late Jurassic-Early Cretaceous transition from
520 marine to non-marine deposits in the eastern segment of the MOO. Meanwhile, the Late
521 Jurassic magmatic rocks in the eastern segment show arc magmatic geochemical
522 affinities, indicating that subduction of the Mongol-Okhotsk oceanic slab was still
523 ongoing in the Late Jurassic and the final closure of the MOO occurred in the Latest
524 Jurassic to Earliest Cretaceous ([Ouyang et al., 2015](#); [Wan et al., 2019](#)).

525 In conclusion, geological evidence mainly supports a Middle-Late Jurassic closure
526 of the MOO ([Figure 9](#)). The inconsistency from different aspects of geological evidence
527 is mainly caused by the range of constraint on the timing of collision. For example,
528 transition from marine to non-marine deposits can constrain the final disappearance of the
529 oceanic basin, however, this age can be much younger than the timing of collision as
530 after continental collision, marine sedimentary basin can still last for long time. For
531 example, after the collision between the Arabian Block and Eurasian continent in the
532 Oligocene, marine deposits preserved until to present day in the Persian Gulf. Therefore,
533 marine to non-marine transition can only provide a loose constraint on the final closure
534 of the MOO. S-type granite represents syn-collision partial melting of thickened lower
535 crust, age of which may be closer to the timing of continental collision. [Li et al. \(2015\)](#)
536 identified a ca. 168 Ma S-type granite in the northern Great Xing'an Range, suggesting
537 a Middle Jurassic closure of the MOO ([Li et al., 2018](#)). Detrital zircon exchange can
538 constrain the upper limit of oceanic closure. [Sorokin et al. \(2020\)](#) found that the Upper
539 Jurassic from both sides of the suture display similar detrital zircon distribution pattern,
540 indicating that detrital zircon exchange has occurred in the Late Jurassic, therefore, the
541 most likely timing for closure of the MOO should be the Middle Jurassic ([Figure 9c](#)).
542 However, paleomagnetic evidence mainly argues for a Late Jurassic-Early Cretaceous
543 closure of the MOO, younger than that concluded from geological evidence. This
544 inconsistency from geological and paleomagnetic aspects should be noticed, and
545 integrated geological and paleomagnetic studies should be performed in the future in

546 order to reach a consistent constraint on the timing of closure of the MOO.



547

548 Figure 9. Bidirectional subduction and closure model of the MOO. (a) Late Permian:
 549 Bidirectional subduction of the Mongol-Okhotsk oceanic slab beneath the southern
 550 margin of the SIB and northern margin of the AMB. In the western segment, the
 551 Mongol-Okhotsk oceanic slab subducted beneath the Tarvagatay Block (TAR). (b) Late
 552 Triassic: Collision between the TAR and AMB caused closure of the western segment
 553 of the MOO; Bidirectional subduction of the Mongol-Okhotsk oceanic slab continued
 554 in the eastern segment. (c) Middle-Late Jurassic: Closure of the MOO in its eastern
 555 segment. Cartons in the left show relative orientations of both the SIB and AMB in
 556 different periods (based on paleogeographic reconstruction in Van der Voo et al., 2015).
 557 The cross-section A-B is located in the Khangay section and the cross-section C-D is
 558 located in the Ergun section of the Mongol-Okhotsk suture.

559 **5. Problems and opportunities about paleomagnetic studies on the evolution of the**

560 **MOO**

561 As a quantitative method constraining paleolatitude and paleogeography of plates,
562 paleomagnetism can play an important role in the study of evolution of the MOO.
563 However, paleomagnetic studies on the evolution of the MOO are insufficient and
564 showing inconsistent or even contradictory results, resulting in the hot debate on this
565 subject. Here, we will analyze possible reasons for this problem and hope this can
566 contribute to the future paleomagnetic studies on the evolution of the MOO.

567 **5.1 Problems about paleomagnetic constraints on the initial closure of the MOO**

568 The initial closure of the MOO in its western segment is the consequence of
569 collision between the northwestern margin of the AMB and Western Mongolian Blocks
570 (Tuva-Mongolia Block and Tarvagatay Block) along the southern margin of the SIB.
571 Available sedimentological and magmatic evidence supports a Late Triassic initial
572 closure of the MOO (Badarch et al., 2002; Wang et al., 2022). However, as there is no
573 Mesozoic paleomagnetic data reported from the Tuva-Mongolia Block and Tarvagatay
574 Block to the north of the suture, or from the AMB to the south of the suture,
575 paleomagnetists used data from the SIB and NCC to constrain the evolution of the
576 MOO and reached a conclusion that the MOO closed simultaneously in the Late
577 Jurassic-Early Cretaceous from west to east (Enkin et al., 1992; Van der Voo et al.,
578 2015). The precondition for this kind of paleomagnetic comparison is that the Tuva-
579 Mongolia Block and Tarvagatay Block stay at the southern margin of the SIB ever since
580 their accretion to the SIB in the Neoproterozoic-Early Paleozoic. However, recent
581 paleomagnetic studies show that after the accretion to the southern margin of the SIB,
582 the Western Mongolian Blocks coevolved with the SIB for a short-time period, and
583 rifted from the SIB since the Silurian and drifted away from the SIB (Kilian et al., 2016).
584 Since the Late Silurian, the SIB drifted northward to high latitude, whereas the Western
585 Mongolian Blocks moved southward to low latitude (Kilian et al., 2016) and reached
586 ca. 25° N during the Late Carboniferous (ca. 315 Ma) close to the AMB (Ren et al.,
587 2021). Due to the lack of Permian paleomagnetic data, the Permian paleoposition of the
588 Western Mongolian Block cannot be constrained. However, as the Late Triassic
589 paleolatitude of the Tarvagatay Block was at $32.8 \pm 16.8^\circ$ N, indicating that the Western

590 Mongolian Blocks still located in low latitude in the Late Triassic (Pruner, 1992). Our
591 new Late Triassic paleomagnetic results confirmed that the Tarvagatay Block located
592 in the paleolatitude of 30-35°N during the Late Triassic, consistent with that of the
593 AMB, suggesting that the western segment of the MOO should have closed in the Late
594 Triassic (Zhao et al., 2023).

595 Therefore, for initial closure of the MOO, one should compare paleolatitudes of
596 the AMB with Western Mongolian Blocks directly rather than with those of the SIB.
597 Future paleomagnetic studies can focus on the Tuva-Mongolia Block and the
598 Tarvagatay Block. From newly obtained Late Paleozoic and Triassic paleomagnetic
599 data, one can constrain the drifting history of the Western Mongolian Blocks and further
600 discuss initial closure of the MOO. Meanwhile, if the Western Mongolian Blocks stayed
601 in low latitude during the Late Paleozoic and Triassic, there must be a big latitudinal
602 difference between the Western Mongolian Blocks and SIB in this period. Does this
603 mean that there was an oceanic basin between them (an independent oceanic basin or a
604 branch of the MOO)? This will be another subject for the evolution of the MOO.

605 **5.2 Effect of the true polar wander (TPW) on the final closure of the MOO**

606 The TPW is due to the reorganization of Earth mass during Earth rotation resulting
607 in rotation of the crust and mantle relative to the liquid outer core. Plates show rapid
608 latitudinal drift and relative rotation during the TPW (Evan, 2003; Steinberger and
609 Torsvik, 2008; Kent and Irving, 2010). The TPW event in the Jurassic resulted in a
610 global clockwise rotation around an Euler pole at western Africa (0°N, 11°E;
611 Steinberger and Torsvik, 2008; Creveling et al., 2012; Torsvik et al., 2012). This TPW
612 was referred as the “monster shift” by Kent et al. (2015). As the SIB and eastern Asian
613 blocks located far away from the Euler pole, the clockwise rotation during this TPW
614 event can result in dramatic southward drift of these blocks (Muttoni and Kent, 2019;
615 Yi et al., 2019; Fu et al., 2020), which will affect the evolution of the MOO. Li (1993)
616 firstly applied the TPW theory to study movement of the NCC during 200-120 Ma and
617 concluded that the Jurassic movement of the NCC was affected by this TPW event. Yi
618 et al. (2019) reported a Middle Jurassic (174 Ma) paleolatitude of the NCC at $61.7^\circ \pm$
619 9.1°N , consistent with that of the SIB. Therefore, they proposed that the MOO should

620 have been closed in the Early and Middle Jurassic boundary, and then the eastern Asian
621 blocks moved southward rapidly about 25° to $36.6^{\circ} \pm 5.1^{\circ}\text{N}$ in the Late Jurassic (157
622 Ma; Yi and Meert, 2020). However, Gao et al. (2021) reported three paleomagnetic
623 poles (170 Ma, 165 Ma and 160Ma) from the Middle-Late Jurassic volcanic rocks in
624 the northern margin of the NCC, which show no obvious latitudinal movement of the
625 NCC, but the SIB moved southward rapidly during this period. This phenomenon was
626 explained as a result of combined influence of the Jurassic TPW and evolution of the
627 MOO (Gao et al., 2021). In the framework of the TPW, both the SIB and the NCC-
628 AMB should move southward rapidly. However, due to the northward subduction of
629 the Mongol-Okhotsk oceanic slab, the dragging force will pull the NCC-AMB
630 northward, which will counteract the TPW-induced southward movement. Therefore,
631 the NCC-AMB shows insignificant movement during this period (Gao et al., 2021).
632 Meanwhile, the paleolatitudes of the SIB and NCC-AMB have already overlapped in
633 the range of uncertainty at 155 Ma (Figure 8), indicating that the MOO should have
634 closed or have limited width.

635 Note that based on the model of Kent et al. (2015), the “monster shift” occurred in
636 the Late Jurassic-Early Cretaceous (160-140 Ma). Therefore, the Early-Middle Jurassic
637 evolution of the MOO should not be affected by this true polar wander event. Due to
638 the lack of paleomagnetic poles in the age of 160-140 Ma for both the SIB and NCC,
639 we cannot evaluate whether the “monster shift” true polar wander affect the plate
640 motions in East Asia or the closure of the MOO. In this case, further paleomagnetic
641 studies are needed for blocks in East Asia. New high-quality Late Jurassic
642 paleomagnetic poles with good age constraints will provide us opportunities to discuss
643 the influence of this true polar wander event to East Asian blocks and closure of the
644 MOO.

645 **6. Conclusion**

646 As the last main ocean that affected the amalgamation and tectonic evolution of
647 northeastern Asia, the MOO separated the SIB to the north, the NCC-AMB to the south
648 and the Western Mongolian Blocks (including Tuva-Mongolia Block, Tarvagatay Block
649 etc.) to the west. The MOO experienced long-term evolution from the Early Paleozoic

650 to Mesozoic. The opening of the MOO can be traced to its early stage at the Early
651 Paleozoic. The northward subduction of the Mongol-Okhotsk oceanic slab beneath the
652 southern margin of the SIB initiated in the Silurian, whereas its southward subduction
653 beneath the north margin of the NCC-AMB started in the Late Devonian, relatively
654 later than the northward one. The bidirectional subduction of the Mongol-Okhotsk
655 oceanic slab resulted in pulse arc magmatism, with three main peaks in the earliest
656 Carboniferous, Late Permian and Late Triassic-Early Jurassic. In the Late Triassic, due
657 to the collision between the AMB and the Western Mongolian Blocks, the ribbon-
658 shaped Western Mongolian Blocks bended and caused the initial closure of the MOO
659 in its western segment. Due to the clockwise rotation of the SIB and counterclockwise
660 one of the NCC-AMB, the MOO showed a scissor-like closure pattern from west to
661 east. The final closure of the MOO occurred in the Middle-Late Jurassic, leading to the
662 formation of the Mongol-Okhotsk orogenic belt, which also resulted in the formation
663 of the Mongol Orocline. Since then, the amalgamation of main blocks in the
664 northeastern Asia has finished, and the northeastern Asian continent went into the
665 intraplate evolutionary stage.

666

667 **Acknowledgements:** We thank Yanyang Wang, Yanjie Zhang, Yan Xu and Liyang
668 Zhang for their assistant in the field, and Zhenhua Jia and Yifei Hou for their help in
669 the paleomagnetic measuring process. We appreciate the Editor and two anonymous
670 reviewers for their constructive suggestions, which improve our manuscript. This study
671 was supported by the National Natural Science Foundation of China (Grant No.
672 92155203).

673

674 **References:**

675 Arzhannikova A V, Demonterova E I, Jolivet M, Arzhannikov S G, Mikheeva E A,
676 Ivanov A V, Khubanov V B, Pavlova L A. 2020. Late Mesozoic topographic
677 evolution of western Transbaikalia: evidence for rapid geodynamic changes from
678 the Mongol-Okhotsk collision to widespread rifting. *Geosci Front* 11: 1695–1709
679 Arzhannikova A V, Demonterova E I, Jolivet M, Mikheeva E A, Ivaanov A V,
680 Arzhannikov S G, Khubanov V B, Kamenetsky V S. 2022. Segmental closure of
681 the Mongol-Okhotsk Ocean: Insight from detrital geochronology in the East

682 Transbaikalia Basin. *Geosci Front* 13: 101254

683 Badarch G, Cunningham W D, Windley B F. 2002. A new block subdivision for
684 Mongolia: implications for the Phanerozoic crustal growth of Central Asia. *J Asian*
685 *Earth Sci* 21: 87–110

686 Bold U, Crowley J, Smith E, Sambuu O, Macdonald F. 2016. Neoproterozoic to early
687 Paleozoic tectonic evolution of the Zavkhan terrane of Mongolia: Implications for
688 crustal growth in the Central Asian orogenic belt. *Lithosphere*, 8: 729-750

689 Buchan C, Cunningham D, Windley B, Tomurhuu D. 2001. Structural and lithological
690 characteristics of the Bayankhongor Ophiolite Zone, Central Mongolia. *J Geol Soc*
691 158(3): 445–460

692 Buchan C, Pfänder J, Kröner A, Brewer T S, Tomurtogoo O, Tomurhuu D, Cunningham
693 D, Windley B F. 2002. Timing of accretion and collisional deformation in the
694 Central Asian Orogenic Belt: Implications of granite geochronology in the
695 Bayankhongor Ophiolite Zone. *Chem Geol* 192: 23–45

696 Bussien D, Gombojav N, Winkler W, Von Quadt A. 2011. The Mongol-Okhotsk Belt in
697 Mongolia—a new appraisal of the geodynamic development by the study of sand-
698 stone provenance and detrital zircons. *Tectonophysics* 510: 132–150

699 Chen L, Liang C, Neubauer F, Liu Y, Zhang Q, Song Z. 2022. Sedimentary processes
700 and deformation styles of the Mesozoic sedimentary succession in the northern
701 margin of the Mohe basin, NE China: Constraints on the final closure of the
702 Mongol–Okhotsk Ocean. *J Asian Earth Sci* 232: 105052

703 Cocks L R M, Torsvik T H. 2007. Siberia, the wandering northern terrane, and its
704 changing geography through the Palaeozoic. *Earth-Sci Rev* 82(1-2): 29-74

705 Cogné J-P, Kravchinsky V, Halim N, Hankard F. 2005. Late Jurassic-Early Cretaceous
706 closure of the Mongol-Okhotsk Ocean demonstrated by new Mesozoic
707 palaeomagnetic results from the Trans-Baikal area (SE Siberia). *Geophys J Int*
708 163(2): 813-832

709 Creveling J R, Mitrovica J X, Chan N H, Latychev K, Matsuyama I. 2012. Mechanisms
710 for oscillatory true polar wander. *Nature* 491: 244-248

711 Donskaya T V, Gladkochub D P, Mazukabzov A M, De Waele B, Presnyakov S L. 2012.
712 The Late Triassic Kataev volcanoplutonic association in western Transbaikalia, a
713 fragment of the active continental margin of the Mongol-Okhotsk Ocean. *Russian*
714 *Geol Geophys* 53(1) : 22-36

715 Donskaya T V, Gladkochub D P, Mazukabzov A M, Ivanov A V. 2013. Late Paleozoic
716 – Mesozoic subduction-related magmatism at the southern margin of the Siberian
717 continent and the 150 million-year history of the Mongol-Okhotsk Ocean. *J Asian*
718 *Earth Sci* 62: 79–97

719 Duan X, Zhou C, Yang H, Cai Y, Wei X, Xu J, Zhao J. 2021. Detrital zircon U-Pb dating
720 and geochemical characteristics of the Ershi'erzhan Formation in western Mohe
721 basin and its provenance significance. *Acta Geologica Sinica* 95(11): 3317-3334

722 Enkin R J, Yang Z Y, Chen Y, Courtillot V. 1992. Paleomagnetic constraints on the
723 geodynamic history of the major blocks of China from the Permian to the present.
724 *J Geophys Res* 97: 13953–13989

725 Evans D A D. 2003. True polar wander and supercontinents. *Tectonophysics* 362: 303-

- 727 Fersman A E. 1926. Mongol–Okhotsk metallic belt. *Surface Bowels* 4, 28–38 (in
728 Russian)
- 729 Ftzell E H, Bull A L, Shephard G E. 2016. Closure of the Mongol–Okhotsk Ocean:
730 Insights from seismic tomography and numerical modelling. *Earth Planet Sci Lett*
731 445: 1–12
- 732 Fu J Y, Na F C, Li Y C, Sun W, Zhong H, Yang H, Yang X P, Zhang G Y, Liu Y C, Yang
733 Y J. 2021. Southward subduction of the Mongo-Okhotsk Ocean: Middle Triassic
734 magmatic records of the “Luomahu Group” in northwest of Lesser Khingan
735 Mountains. *Geol Bull China* 40(6): 889-904
- 736 Fu R R, Kent D V, Hemming S R, Gutiérrez P, Creveling J R. 2020. Testing the
737 occurrence of Late Jurassic true polar wander using the La Negra volcanics of
738 northern Chile. *Earth Planet Sci Lett* 529: 115835
- 739 Gordienko I V, Metelkin D V, Vetluzhskikh L .I. 2019. The Structure of the Mongol-
740 Okhotsk Fold Belt and the Problem of Recognition of the Amur Microcontinent.
741 *Russian Geol Geophys* 60: 267-286
- 742 Hankard F, Cogne J-P, Kravchinsky V. 2005. A new Late Cretaceous paleomagnetic
743 pole for the west of Amuria block (Khurmen Uul, Mongolia). *Earth Planet Sci Lett*
744 236(1-2): 359-373
- 745 Halim N, Kravchinsky V, Gilder S, Conge J-P, Alexyutin M, Sorokin A, Coutillot V,
746 Chen Y. 1998. A palaeomagnetic study from the Mongol–Okhotsk region: rotated
747 Early Cretaceous volcanics and remagnetized Mesozoic sediments. *Earth Planet*
748 *Sci Lett* 159: 133-145
- 749 He Z J, Li J Y, Mo, S G, Sorokin A A. 2005. Geochemical discriminations of sandstones
750 from the Mohe Foreland basin, northeastern China: tectonic setting and
751 provenance. *Science in China Series D Earth Sciences* 48 (5): 613–621
- 752 Janoušek V, Jiang Y, Buriánek D, Schulmann K, Hanžl P, Soejono I, Kröner A,
753 Altanbaatar B, Erban V, Lexa O, Ganchuluun T, Košler J. 2018. Cambrian–
754 Ordovician magmatism of the Ikh–Mongol Arc System exemplified by the
755 Khantaishir Magmatic complex (Lake Zone, south–Central Mongolia). *Gondwana*
756 *Res* 54: 122–149
- 757 Ji Z, Ge W C, Yang H, Bi J H, Yu Q, Dong Y. 2018. The Late Trassic Andean-type
758 andesite from the central Great Xing’an Range: Products of the southward
759 subduction of the Mongol-Okhotsk oceanic plate. *Acta Petrol Sinica* 34(10): 2917-
760 2930
- 761 Jian P, Kröner A, Windley B F, Shi Y, Zhang F, Miao L, Tomurhuu D, Zhang W, Liu D.
762 2010. Zircon ages of the Bayankhongor ophiolite mélange and associated rocks:
763 Time constraints on Neoproterozoic to Cambrian accretionary and collisional
764 orogenesis in Central Mongolia. *Precambrian Res* 177(1–2): 162–180
- 765 Kashiwagi K, Tsukada K, Minjin C. 2004. Paleozoic spherical radiolarians from the
766 Gorkhi Formation, southwest Khentei range, central Mongolia; a preliminary
767 report. *Mongolian Geoscientist* 24: 17–26
- 768 Kelty T K, Yin A, Dash B, Gehrels G E, Ribeiro A E. 2008. Detrital-zircon
769 geochronology of Paleozoic sedimentary rocks in the Hangay–Hentey basin,

770 north-central Mongolia: implications for the tectonic evolution of the Mongol-
771 Okhotsk Ocean in central Asia. *Tectonophysics* 451: 290-311

772 Kent D V, Irving E. 2010. Influence of inclination error in sedimentary rocks on the
773 Triassic and Jurassic apparent pole wander path for North America and
774 implications for Cordilleran tectonics. *J Geophys Res* 115: [https:// doi.org](https://doi.org/10.1029/2009JB007205)
775 /10.1029/2009JB007205.

776 Kent, D V, Kjarsgaard B A, Gee J S, Muttoni G, Heaman L M. 2015. Tracking the Late
777 Jurassic apparent (or true) polar shift in U-Pb-dated kimberlites from cratonic
778 North America (Superior Province of Canada). *Geochem Geophys, Geosyst* 16:
779 983-994

780 Khanchuk A I, Didenko A N, Popeko L I, Sorokin A A, Shevchenko B F. 2015. Structure
781 and Evolution of the Mongol-Okhotsk Orogenic Belt, in Kröner, A., eds., *The*
782 *Central Asian Orogenic Belt. Geology, Evolution, Tectonics, and Models.*
783 *Borntraeger Science Publishers, Stuttgart, Germany, 211–234.*

784 Kilian T M, Swanson-Hysell N L, Bold U, Crowley J, Macdonald F A. 2016.
785 Paleomagnetism of the Teel basalts from the Zavkhan terrane: Implications for
786 Paleozoic paleogeography in Mongolia and the growth of continental crust.
787 *Lithosphere* 8, 699-715

788 Kravchinsky V A, Sorokin A A, Courtillot V. 2002a. Paleomagnetism of Paleozoic and
789 Mesozoic sediments from the southern margin of Mongol-Okhotsk ocean, far
790 eastern Russia. *J Geophys Res* 107 (B10), 2253

791 Kravchinsky V A, Cogné J-P, Harbert W P, Kuzmin M I. 2002b. Evolution of the
792 Mongol–Okhotsk Ocean as constrained by new palaeomagnetic data from the
793 Mongol–Okhotsk suture zone, Siberia. *Geophys J Int* 148: 34-57

794 Kurihara T, Tsukada K, Otoh S, Kashiwagi K, Chuluun M, Byambadash D, Boijir B,
795 Gonchigdorj S, Nuramkhan M, Niwa M, Tokiwa T, Hikchi G, Kozuka T. 2009.
796 Upper Silurian and Devonian pelagic deep-water radiolarian chert from the
797 Khangai–Khentei belt of Central Mongolia: Evidence for Middle Paleozoic
798 subduction–accretion activity in the Central Asian Orogenic Belt. *J Asian Earth*
799 *Sci* 34: 209–225

800 Kuzmin M I, Kravchinsky V A. 1996. Preliminary paleomagnetic data on the
801 Mongolia–Okhotsk fold belt. *Russian Geol Geophys* 37 (1): 54–62

802 Li J Y, 2006. Permian geodynamic setting of Northeast China and adjacent regions:
803 closure of the Paleo-Asian Ocean and subduction of the Paleo-Pacific Plate. *J*
804 *Asian Earth Sci* 26: 207–224

805 Li P. 1993. Interpretation of Mesozoic crustal movements in North China-Ture polar
806 wander model. *Geol Rev* 39(5): 390-394

807 Li Y, Ding L L, Xu W L, Wang F, Tang J, Zhao S, Wang Z J. 2015. Geochronology and
808 geochemistry of muscovite granite in Sunwu area, NE China: Implication for the
809 timing of closure of the Mongol-Okhotsk Ocean. *Acta Petrol Sinica* 31(1): 56-66

810 Ling J, Li P, Yuan C, Sun M, Zhang Y, Narantsetseg T, Wang X, Jiang Y, Hu W. 2021.
811 Ordovician to Devonian granitic plutons in the Hangay Range, Central Mongolia:
812 Petrogenesis and insights into the Paleozoic tectonic evolution of the westernmost
813 Mongol-Okhotsk Orogen. *Lithos* 404-405: 106463

- 814 Li P, Sun M, Narantsetseg T, Jourdan F, Hu W, Yuan C. 2022. First structural
815 observation around the hinge of the Mongolian Orocline (Central Asia):
816 Implications for the geodynamics of oroclinal bending and the evolution of the
817 Mongol-Okhotsk Ocean. *Geol Soc Am Bull* 134: 1994-2006
- 818 Li Y, Xu W-L, Wang F, Tang J, Zhao S, Guo P. 2017a. Geochronology and geochemistry
819 of late Paleozoic–early Mesozoic igneous rocks of the Erguna Massif, NE China:
820 Implications for the early evolution of the Mongol–Okhotsk tectonic regime. *J*
821 *Asian Earth Sci* 144: 205–224
- 822 Li Y, Xu W-L, Wang F, Pei F P, Tang J, Zhao S. 2017b. Triassic volcanism along the
823 eastern margin of the Xing'an Massif, NE China: Constraints on the spatial–
824 temporal extent of the Mongol–Okhotsk tectonic regime. *Gondwana Res* 48: 205-
825 223
- 826 Li Y, Xu W-L, Tang J, Pei F P, Wang F, Sun C Y. 2018. Geochronology and
827 geochemistry of Mesozoic intrusive rocks in the Xing'an Massif of NE China:
828 Implications for the evolution and spatial extent of the Mongol–Okhotsk tectonic
829 regime. *Lithos* 304-307: 57-73
- 830 Liu Y, Li W, Ma Y, Feng Z, Guan Q, Li S, Chen Z, Liang C, Wen Q. 2021. An orocline
831 in the eastern Central Asian Orogenic Belt. *Earth Sci Rev* 221: 103808
- 832 Ma X, Xing L, Yang Z, Xu S, Zhang J. 1993. Paleomagnetic study since late Paleozoic
833 in the Ordos Basin. *Acta Geophys Sinica* 36(1): 68-79
- 834 McDannell K T, Zeitler P K, Idleman B D. 2018. Relict topography within the Hangay
835 Mountains in central Mongolia: Quantifying long-term exhumation and relief
836 change in an old landscape. *Tectonics* 37: 2531–2558
- 837 Meng Q R, Wu G L, Fan L G, Wei H H, Wang E. 2020. Late Triassic uplift, magmatism
838 and extension of the northern North China block: Mantle signatures in the surface.
839 *Earth Planet Sci Lett* 547: 116451
- 840 Metelkin D V, Vernikovskiy V A, Kazansky AYu, Wingate M T D. 2010. Late Mesozoic
841 tectonics of Central Asia based on paleomagnetic evidence. *Gondwana Res* 18(2-
842 3): 400-419
- 843 Minjin Ch, Tomurtogoo O, Dorjsuren B, 2006. Devonian-Carboniferous accretionary
844 complex of the Ulaanbaatar terrane. In: Tomurhuu, D., Natal'in, B.A.,
845 Ariunchimeg, Y., Khishigsuren, S., Erdenesaikhan, G. (Eds.), *Structural and*
846 *Tectonic Correlation across the Central Asia Orogenic Collage: Implications for*
847 *Continental Growth and Intracontinental Deformation (Second International*
848 *Workshop and Field Excursions for IGC Project 480)*, abstract and excursion
849 guidebook, pp. 100–106.
- 850 Muttoni G, Kent D V, 2019. Jurassic Monster Polar Shift Confirmed by Sequential
851 Paleopoles From Adria, Promontory of Africa. *J Geophys Res: Solid Earth* 124:
852 3288-3306
- 853 Narantsetseg T, Orolmaa D, Yuan C, Wang T, Guo L, Tong Y, Wang X, Enkh-Orshikh
854 O, Oyunchimeg T-U, Delgerzaya P, Enkhdalai B. 2019. Early-Middle Paleozoic
855 volcanic rocks from the Ereendavaa terrane (Tsarigiin gol area, NE Mongolia)
856 with implications for tectonic evolution of the Kherlen massif. *J Asian Earth Scis*
857 175: 138–157

858 Natal'in B, 1993. History and modes of Mesozoic accretion in Southeastern Russia.
859 Island Arc 2: 15–34

860 Osozawa S, Tsolmon G, Majigsuren U, Sereenen J, Niitsuma S, Iwata N, Pavlis T, Jahn
861 B M. 2008. Structural evolution of the Bayanhongor region, west-central
862 Mongolia. *J Asian Earth Sci* 33(5): 337–352

863 Ovchinnikov R O, Sorokin A A, Xu W L, Kudryashov N M. 2023. Late Paleozoic and
864 early Mesozoic granitoids in the northwestern Bureya Massif, Central Asian
865 Orogenic Belt: Timing and tectonic significance. *Int Geol Rev* DOI:
866 10.1080/00206814.2023.2178035

867 Ouyang H G, Mao J W, Zhou Z H, Su H M. 2015. Late Mesozoic metallogeny and
868 intracontinental magmatism, southern Great Xing'an Range, northeastern China.
869 *Gondwana Res* 27: 1153–1172

870 Parfenov L M, Popeko L I, Tomurtogoo O. 2001. Problems of tectonics of the Mongol-
871 Okhotsk Orogenic Belt. *Geology of Pacific Ocean* 16 (5): 797–830

872 Parfenov L M, Badarch G, Berzin N A, Khanchuk A I, Kuzmin M I, Nokleberg W J,
873 Prokopiev A V, Ogasawara M, Yan H. 2009. Summary of Northeast Asia
874 geodynamics and tectonics. *Stephan Mueller Spec. Publ. Ser.*, 4: 11–33

875 Pei J L, Sun Z M, Liu J, Liu J, Wang X S, Yang Z Y, Zhao Y, Liu H B. 2011. A
876 paleomagnetic study from the Late Jurassic volcanics (155 Ma), North China:
877 implications for the width of Mongol–Okhotsk Ocean. *Tectonophysics* 510: 370–
878 380

879 Pruner P. 1987. Palaeomagnetism and palaeogeography of Mongolia in the Cretaceous,
880 Permian and Carboniferous-preliminary data. *Tectonophysics* 139: 155-167

881 Pruner P. 1992. Palaeomagnetism and palaeogeography of Mongolia from the
882 Carboniferous to the Cretaceous-final report. *Phys Earth Planetary Inter* 70: 169–
883 177

884 Ren Q, Zhang S, Wu H, Liang Z, Miao X, Zhao H, Li H, Yang T, Pei J, Davis G A.
885 2016. Further paleomagnetic results from the ~ 155 Ma Tiaojishan Formation,
886 Yanshan Belt, North China, and their implications for the tectonic evolution of the
887 Mongol–Okhotsk suture. *Gondwana Res* 35: 180-191

888 Ren Q, Zhang S, Wu Y, Yang T, Gao Y, Turbold S, Zhao H, Wu H, Li H, Fu H, Xu B,
889 Zhang J, Tomurtogoo O. 2018. New Late Jurassic to Early Cretaceous
890 Paleomagnetic Results From North China and Southern Mongolia and Their
891 Implications for the Evolution of the Mongol-Okhotsk Suture. *J Geophys Res:*
892 *Solid Earth* 123(12): 10,370-310,398

893 Ren Q, Zhang S, Sukhbaatar T, Zhao H, Wu H, Yang T, Li H, Gao Y, Jin X. 2021. Did
894 the Boreal Realm extend into the equatorial region? New paleomagnetic evidence
895 from the Tuva–Mongol and Amuria blocks. *Earth Planet Sci Lett* 576: 117246

896 Ruppen D, Knaf A, Bussien D, Winkler W, Chimedtseren A, von Quadt A. 2014.
897 Restoring the Silurian to Carboniferous northern active continental margin of the
898 Mongol–Okhotsk Ocean in Mongolia: Hangay–Hentey accretionary wedge and
899 seamount collision. *Gondwana Res* 25(4): 1517-1534

900 Serezhnikov A N, Volkova Yu R. 2007. State Geological Map of the Russian Federation.
901 Third Generation. Far East Series. Scale 1:000 000. Sheet N-52, Zeya. Vol'skii,

- 902 A.S., Eds. St. Petersburg, VSEGEI.
- 903 Sheldrick T C, Barry T L, Millar I L, Barfod D N, Halton A M, Smith D J. 2020.
904 Evidence for southward subduction of the Mongol-Okhotsk oceanic plate:
905 implications from Mesozoic adakitic lavas from Mongolia. *Gondwana Res* 79:
906 140-156
- 907 Smirnova Y N, Sorokin A, Popeko L, Kotov A, Kovach V P. 2017. Geochemistry and
908 provenances of the Jurassic terrigenous rocks of the Upper Amur and Zeya–Dep
909 troughs, eastern Central Asian fold belt. *Geochem Inter* 55(2): 163–183
- 910 Sorokin A A, Kotov A B, Sal’nikova E B, Kudryashov N M, Kovach V P. 2007. Early
911 Paleozoic gabbro-granitoid associations in eastern segment of the Mongolian-
912 Okhotsk foldbelt (Amur River basin): Age and tectonic position. *Stratigraphy and
913 Geological Correlation* 15(3): 241-257
- 914 Sorokin A A, Kotov A B, Kudryashov N M, Kovach V P. 2015. First evidence of
915 Ediacaran magmatism in the geological history of the Mamyn Terrane of the
916 Central Asian fold belt. *Russian Journal of Pacific Geology* 9(6): 399-410.
- 917 Sorokin A A, Kudryashov N M, Kotov A B, Kovach V P. 2017. Age and tectonic setting
918 of the early Paleozoic magmatism of the Mamyn Terrane, Central Asian Orogenic
919 Belt, Russia. *J Asian Earth Sci* 144: 22-39
- 920 Sorokin A A, Zaika V A, Kovach V P, Kotov A B, Xu W, Yang H. 2020. Timing of
921 closure of the eastern Mongol–Okhotsk Ocean: Constraints from U–Pb and Hf
922 isotopic data of detrital zircons from metasediments along the Dzhagdy Transect.
923 *Gondwana Res* 81: 58-78
- 924 Sorokin A A, Zaika V A, Kudryashov N M. 2021. Timing of formation and tectonic
925 setting of Paleozoic granitoids in the eastern Mongol–Okhotsk Belt: Constraints
926 from geochemical, U Pb, and Hf isotope data. *Lithos* 388-389: 106086
- 927 Steinberger B, Torsvik T H. 2008. Absolute plate motions and true polar wander in the
928 absence of hotspot tracks. *Nature* 452: 620-623
- 929 Sun D Y, Gou J, Wang T H, Ren Y S, Liu Y J, Guo H Y, Liu X M, Hu Z C. 2013.
930 Geochronological and geochemical constraints on the Erguna massif basement,
931 NE China—subduction history of the Mongol-Okhotsk oceanic crust. *Inter Geol
932 Rev* 55: 1801-1816
- 933 Tang J, Xu W-L, Wang F, Wang W, Xu M J, Zhang Y H. 2013. Geochronology and
934 geochemistry of Neoproterozoic magmatism in the Erguna Massif, NE China:
935 Petrogenesis and implications for the breakup of the Rodinia supercontinent.
936 *Precambrian Res* 224: 597-611
- 937 Tang J, Xu W-L, Wang F, Wang W, Xu M, Zhang Y. 2014. Geochronology and
938 geochemistry of Early–Middle Triassic magmatism in the Erguna Massif, NE
939 China: Constraints on the tectonic evolution of the Mongol–Okhotsk Ocean.
940 *Lithos* 184-187: 1-16
- 941 Tang J, Xu W-L, Wang F, Zhao S, Li Y. 2015. Geochronology, geochemistry, and
942 deformation history of Late Jurassic–Early Cretaceous intrusive rocks in the
943 Erguna Massif, NE China: Constraints on the late Mesozoic tectonic evolution of
944 the Mongol–Okhotsk orogenic belt. *Tectonophysics* 658: 91-110
- 945 Tang J, Xu W-L, Wang F, Zhao S, Wang W. 2016. Early Mesozoic southward

946 subduction history of the Mongol–Okhotsk oceanic plate: Evidence from
947 geochronology and geochemistry of Early Mesozoic intrusive rocks in the Erguna
948 Massif, NE China. *Gondwana Res* 31: 218–240

949 Tang J, Xu W L, Wang F, Ge W C. 2018. Subduction history of the Paleo-Pacific slab
950 beneath Eurasian continent: Mesozoic-Paleogene magmatic records in Northeast
951 Asia. *Sci China Earth Sci* 48(5): 549-583

952 Tomurtogoo O, Windley B F, Kroner A, Badarch G, Liu D Y. 2005. Zircon age and
953 occurrence of the Adaatsag ophiolite and Muron shear zone, central Mongolia:
954 constraints on the evolution of the Mongol–Okhotsk ocean, suture and orogen. *J*
955 *Geol Soc* 162: 125-134

956 Torsvik T H, Van der Voo R, Preeden U, Mac Niocaill C, Steinberger B, Doubrovine P
957 V, van Hinsbergen D J J, Domeir M, Gaina C, Tohver E, Meert J G, McCausland
958 P J A, Cocks R M. 2012. Phanerozoic polar wander, paleogeography and dynamics.
959 *Earth-Sci Rev* 114: 325–368

960 Torsvik T, Cocks L. 2016. *Earth History and Palaeogeography*. Cambridge: Cambridge
961 University Press. doi:10.1017/9781316225523

962 Turbin M T, (Ed.), *Decisions of IV Inter-Organizational Regional Stratigraphic Meeting*
963 *for Precambrian and Phanerozoic Epoch at south of far east and eastern Trans-*
964 *Baikalia, (in Russian), 124 pp., Khabarovsk State Mine-Geol. Co. House,*
965 *Khabarovsk, Russia, 1994.*

966 van der Meer D G, van Hinsbergen D J J, Spakman W. 2018. Atlas of the underworld:
967 Slab remnants in the mantle, their sinking history, and a new outlook on lower
968 mantle viscosity. *Tectonophysics* 723: 309-448

969 van der Voo R, Spakman W, Bijwaard H. 1999. Mesozoic subducted slabs under Siberia.
970 *Nature* 397: 246–249

971 Van der Voo R, van Hinsbergen D J J, Domeier M, Spakman W, Torsvik T H. 2015.
972 Latest Jurassic–earliest Cretaceous closure of the Mongol-Okhotsk Ocean: A
973 paleomagnetic and seismological-tomographic analysis, in Anderson, T.H.,
974 Didenko, A.N., Johnson, C.L., Khanchuk, A.I., and MacDonald, J.H., Jr., eds.,
975 *Late Jurassic Margin of Laurasia-A Record of Faulting Accommodating Plate*
976 *Rotation*. Geological Society of America Special Paper 513, 589–606.

977 Walderhaug H J, Eide E A, Scott R A, Inger S, Golionko E G. 2005. Palaeomagnetism
978 and $^{40}\text{Ar}/^{39}\text{Ar}$ geochronology from the South Taimyr igneous complex, Arctic
979 Russia: a Middle–Late Triassic magmatic pulse after Siberian flood-basalt
980 volcanism. *Geophys J Inter* 163: 501–517

981 Wan L, Lu C, Zeng Z, Mohammed A S, Liu Z, Dai Q, Chen K. 2019. Nature and
982 significance of the late Mesozoic granitoids in the southern Great Xing’an range,
983 eastern Central Asian Orogenic Belt. *Inter Geol Rev* 61: 584–606

984 Wang T, Tong Y, Xiao W, Guo L, Windley B F, Donskaya T, Li S, Tserendash N, Zhang
985 J. 2022. Rollback, scissor-like closure of the Mongol-Okhotsk Ocean and
986 formation of an orocline: magmatic migration based on a large archive of age data.
987 *Natl Sci Rev* 9(5): nwab210

988 Wang T, Guo L, Zhang L, Yang Q, Zhang J, Tong Y, Ye K. 2015. Timing and evolution
989 of Jurassic–Cretaceous granitoid magmatisms in the Mongol–Okhotsk belt and

990 adjacent areas, NE Asia: Implications for transition from contractional crustal
991 thickening to extensional thinning and geodynamic settings. *J Asian Earth Sci* 97:
992 365–392

993 Wu H, Zhu R, Liu C, Chang C. 1990. Paleomagnetic observations in North China Block:
994 from Late Paleozoic to Triassic. *Acta Geophys Sinica* 33(6): 694-701

995 Xiao W, Windley B F, Han C, Liu W, Wan B, Zhang J, Ao S, Zhang Z, Song D. 2018.
996 Late Paleozoic to early Triassic multiple roll-back and oroclinal bending of the
997 Mongolia collage in Central Asia. *Earth-Sci Rev* 186: 94-128

998 Xu W L, Pei F P, Wang F, Meng E, Ji W Q, Yang D B, Wang W. 2013a. Spatial–temporal
999 relationships of Mesozoic volcanic rocks in NE China: Constraints on tectonic
1000 overprinting and transformations between multiple tectonic regimes. *J Asian Earth*
1001 *Sci* 74: 167–193

1002 Xu W L, Wang F, Pei F P, Meng E, Tang J, Xu M J, Wang W. 2013b. Mesozoic tectonic
1003 regimes and regional ore-forming background in NE China: Constraints from
1004 spatial and temporal variations of Mesozoic volcanic rock associations. *Acta*
1005 *Petrol Sinica* 29(2): 339-353

1006 Yang Y T, Guo Z X, Song C C, Li X B, He S. 2015. A short-lived but significant
1007 Mongol–Okhotsk collisional orogeny in latest Jurassic–earliest Cretaceous.
1008 *Gondwana Res* 28: 1096–1116

1009 Yang Z, Ma X, Besse J, Courtillot V, Xing L, Xu S, Zhang J. 1991. Paleomagnetic
1010 results from Triassic sections in the Ordos Basin, North China. *Earth Planetary Sci*
1011 *Lett* 104: 258-277

1012 Yi Z, Liu Y, Meert J. 2019. A true polar wander trigger for the Great Jurassic East Asian
1013 Aridification. *Geology* 47(12): 1112-1116

1014 Yi Z, Meert J G. 2020. A closure of the Mongol-Okhotsk Ocean by the Middle Jurassic:
1015 Reconciliation of paleomagnetic and geological evidence. *Geophys Res Lett* 47:
1016 e2020GL088235.

1017 Zaika V A, Sorokin A A, Xu B, Kotov A B, Kovach V P. 2018. Geochemical Features
1018 and Sources of Metasedimentary Rocks of the Western Part of the Tukuringra
1019 Block of the Mongol–Okhotsk Fold Belt. *Stratigraphy and Geological Correlation*
1020 26: 157–178

1021 Zhang Y. 2011. Main Characteristics of Late Jurassic-Cretaceous Tectonic Framework
1022 in Northeast Asia. *J Jilin University (Earth Sci Edition)* 41(5): 1267-1284

1023 Zhao P, Xu B, Jahn B M. 2017. The Mongol-Okhotsk Ocean subduction-related
1024 Permian peraluminous granites in northeastern Mongolia: Constraints from zircon
1025 U-Pb ages, whole-rock elemental and Sr-Nd-Hf isotopic compositions. *J Asian*
1026 *Earth Sci* 144: 225–242

1027 Zhao P, Appel E, Deng C, Xu B. 2023. Bending of the western Mongolian blocks
1028 initiated the Late Triassic closure of the Mongol-Okhotsk Ocean and formation of
1029 the Tuva-Mongol Orocline. *Tectonics* 42(5): e2022TC007475,
1030 <https://doi.org/10.1029/2022TC007475>.

1031 Zhao P, Jia Z, Xu B, Sukhbaatar T, Appel E, Chen Y. 2023. Late Triassic initial closure
1032 of the Mongol-Okhotsk Ocean in the western segment: constraints from
1033 sedimentology, detrital zircon ages and paleomagnetic evidence. *Gondwana Res*

1034 [under review.](#)

1035 Zhao X, Coe R S, Zhou Y, Wu H, Wang J. 1990. New paleomagnetic results from
1036 northern China: collision and suturing with Siberia and Kazakhstan.
1037 *Tectonophysics* 181: 43-81

1038 Zhao X, Coe R S, Gilder S A, Frost G M. 1996. Palaeomagnetic constraints on the
1039 palaeogeography of China: implications for Gondwanaland. *Australian J Earth Sci*
1040 43: 643-672

1041 Zhu M, Zhang F, Miao L, Baatar M, Anaad C, Yang S H, Li X B. 2018. The late
1042 Carboniferous Khuhu davaa ophiolite in northeastern Mongolia: Implications for
1043 the tectonic evolution of the Mongol-Okhotsk ocean. *Geol J* 53: 1263-1278

1044 Zhu M, Pastor-Galan D, Miao L, Zhang F, Ganbat A, Li S, Yang S, Wang Z. 2023a.
1045 Evidence for early Pennsylvanian subduction initiation in the Mongol–Okhotsk
1046 Ocean from the Adaatsag ophiolite (Mongolia). *Lithos* 436-437: 106951

1047 Zhu M, Zhang F, Smit M A, Pastor-Galan D, Guilmette C, Miao L, Zou Y, Yang S,
1048 Ganbat A, Tual L, Wang Z. 2023b. Discovery of a >1,000 km Cambrian Eclogite-
1049 Bearing High-Pressure Metamorphic Belt in the Central Asian Orogenic Belt:
1050 Implications for the Final Closure of the Pan-Rodinian Ocean. *J Geophys Res:*
1051 *Solid Earth* 128(1): doi: 10.1029/2022JB025388.

1052 Zeng W S, Zhou J B, Dong C, Cao J L, Wang B. 2014. Subduction record of Mongol-
1053 Okhotsk Ocean: Constrains from Badaguan metamorphic complexes in the Erguna
1054 massif, NE China[J]. *Acta Petrol Sinica* 30(7): 1948-1960

1055 Zonenshain L P, Kuzmin M I, Natapov L M. 1990. Geology of the USSR: plate tectonic
1056 synthesis. *American Geophysical Union Geodynamics Series* 21: 1-242

1057 Zorin Y A, Belichenko V G, Turutanov E K, Mazukabzov A M, Sklyarov E V,
1058 Mordvinova V V. 1995. The East Siberia Transect. *Int Geol Rev* 37,: 154–175

1059 Zorin Y A. 1999. Geodynamics of the western part of the Mongolia–Okhotsk collisional
1060 belt, Trans-Baikal region (Russia) and Mongolia. *Tectonophysics* 306: 33–56

1061

1062